

A High Resolution Search for Dual AGNs in Mergers: Pushing the Frontier with Keck AO

CAMILO VAZQUEZ ^{1,*} S. SATYAPAL ¹ G. CANALIZO ² N. J. SECREST ³ R. W. PFEIFLE ^{4,†} T. BOHN ⁵
K. NYLAND ⁶ A. ARAVINDAN ² L. BLECHA ⁷ J. M. CANN ^{4,8,†} S. DOAN ¹ E. K. S. HICKS ⁹
P. KURCZYNSKI ¹⁰ S. JUNEAU ¹¹ M. MALKAN ¹² M. McDONALD ² J. MCKAIG ^{4,8} P. NAIR ¹³
B. ROTHBERG ^{1,14} E. SCHWARTZMAN ⁶ F. MULLER-SANCHEZ ¹⁵ R. SEXTON ^{1,3} AND V. U ^{16,17}

¹Department of Physics and Astronomy, George Mason University, MS3F3, 4400 University Drive, Fairfax, VA 22030, USA

²Department of Physics and Astronomy, University of California, Riverside, 900 University Avenue, Riverside, CA 92521, USA

³U.S. Naval Observatory, 3450 Massachusetts Avenue NW, Washington, DC 20392-5420, USA

⁴X-ray Astrophysics Laboratory, NASA Goddard Space Flight Center, Code 662, Greenbelt, MD 20771, USA

⁵Research Center for Space and Cosmic Evolution, Ehime University, Bunkyo-cho 2-5, Matsuyama, Ehime 790-8577, Japan

⁶U.S. Naval Research Laboratory, 4555 Overlook Ave. SW, Washington, DC 20375, USA

⁷Department of Physics, University of Florida, 2001 Museum Rd., Gainesville, FL 32611, USA

⁸Oak Ridge Associated Universities, NASA NPP Program, Oak Ridge, TN 37831, USA

⁹Department of Physics and Astronomy, University of Alaska Anchorage, Anchorage, AK 99508-4664, USA

¹⁰Astrophysics Science Division Code 660, NASA Goddard Space Flight Center, Greenbelt MD 207781, USA

¹¹NSF's National Optical-Infrared Astronomy Research Laboratory, 950 N. Cherry Avenue, Tucson, AZ 85719, USA

¹²Department of Physics & Astronomy, 430 Portola Plaza, University of California, Los Angeles, CA 90095, USA

¹³Department of Physics and Astronomy, The University of Alabama, Tuscaloosa, AL 35487, USA

¹⁴LBT Observatory, University of Arizona, 933 N. Cherry Ave, Tucson AZ 85721, USA

¹⁵Department of Physics and Materials Science, The University of Memphis, 3720 Alumni Avenue, Memphis, TN 38152, USA

¹⁶IPAC, Caltech, 1200 E. California Blvd., Pasadena, CA 91125, USA

¹⁷Department of Physics and Astronomy, 4129 Frederick Reines Hall, University of California, Irvine, CA 92697, USA

ABSTRACT

Accreting supermassive black holes (SMBHs) in galaxy mergers with separations < 1 kpc are crucial to our understanding of SMBH growth, galaxy evolution, and the evolution of SMBH binaries. Despite their importance, there are less than a handful known, and most have been discovered serendipitously. In this work, we employ a new selection method to systematically pre-select candidate advanced mergers likely to contain unresolved substructure at sub-arcsecond scales. By exploiting the large survey area and astrometric precision of the Wide-field Infrared Survey Explorer (WISE) and the Sloan Digital Sky Survey (SDSS), we have identified a sample of 48 nearby advanced mergers that have red WISE colors ($W_1 - W_2 > 0.5$) indicative of accretion activity and significant sub-arcsecond offsets between their optical and infrared coordinates as measured by SDSS and WISE. We conducted high resolution adaptive optics (AO) observations of this sample with the Keck NIRC2 camera in the K_p band ($2.124 \mu\text{m}$, $\Delta\lambda = 0.351 \mu\text{m}$) to search for evidence of previously unresolved substructure suggested by the optical-to-infrared offsets. We find that a significant fraction (20/48 or 42%) of the sample shows substructure tracing the SDSS/WISE offset and unresolved by SDSS, demonstrating that our methodology is a promising pathway to find dual AGN in follow-up spectroscopy. Archival optical Hubble Space Telescope (HST) imaging reveals that substructure identified with Keck is often missed in the optical or erroneously identified due to partial obscuration, underscoring the importance of carrying out studies of late-stage mergers in the infrared.

1. INTRODUCTION

Accreting supermassive black holes (SMBHs) in galaxy mergers with separations < 1 kpc are a natural consequence of the current cosmological paradigm, and capture a key phase in galaxy evolution when the central black holes experience their most rapid growth (Van Wassenhove et al. 2012; Capelo et al. 2015, 2017; Blecha et al. 2018; Chen et al. 2023a). SMBH pairs at these separations are also the more observationally

Corresponding author: Camilo Vazquez
cvazquez4@gmu.edu

* Presidential Scholar

† NASA Postdoctoral Program Fellow

accessible precursors to binary SMBHs, which can give rise to the loudest gravitational wave events in the universe (Merritt & Milosavljević 2005). Despite decades of searching, however, dual accreting SMBHs are extremely rare, most are discovered serendipitously, and the vast majority of advanced mergers have nuclear pair separations that are > 1 kpc (Satyapal et al. 2017), leaving a major gap in our understanding of black hole growth, galaxy evolution, and binary SMBH formation. Relatively few dual AGNs are found to have projected physical separations of < 10 kpc (e.g. Bianchi et al. 2008; Fu et al. 2011b; Koss et al. 2012; Liu et al. 2013; Comerford et al. 2015; Müller-Sánchez et al. 2015; Satyapal et al. 2017; Hou et al. 2019; Pfeifle et al. 2019b), and only one robustly confirmed triple AGN at < 10 kpc has been reported in the literature (Liu et al. 2019; Pfeifle et al. 2019a). Even fewer dual AGNs are found with sub-kpc separations (e.g. 900 pc, Komossa et al. 2003; 767 pc, U et al. (2013), Iwasawa et al. (2018); 620 pc, Müller-Sánchez et al. 2015; 500 pc, Voggel et al. 2022; 230 pc, Koss et al. 2023), and only a single binary AGN has been confirmed (e.g. 7.3 pc, Rodriguez et al. 2006).

With such a small and heterogeneously selected sample, it is impossible to assess their frequency and constrain their properties (Pfeifle et al. 2024), particularly those with pair separations < 1 kpc. Such constraints are critical not only for advancing our understanding of galaxy evolution and black hole growth, but also for improving predictions of SMBH merger rates detectable by future gravitational wave observatories. The frequency of dual AGNs at separations below ~ 1 kpc provides crucial constraints on the evolutionary pathways of binary supermassive black holes (BSBHs), which are thought to eventually merge and contribute to the low-frequency gravitational wave background detected by NANOGrav (Agazie et al. 2023). The orbital evolution of dual and binary SMBHs proceeds through several stages: their separation initially decreases to ~ 10 parsecs via dynamical friction with gas and stars. Below ~ 10 parsecs, the SMBHs become gravitationally bound and continue to inspiral through three-body interactions, interactions with a circumnuclear gas disk at sub-parsec scales, and ultimately gravitational wave emission. The efficiency of dynamical friction, particularly between 1 and 0.1 kpc, is a key factor in setting merger timescales (Kelley et al. 2017; Li et al. 2021, 2022). This underscores the importance of measuring the occurrence rate of dual SMBHs as a function of separation to enable more robust predictions for the gravitational wave background.

Directly identifying BSBHs with parsec-scale separations is beyond the resolution of any facility, including the Very Large Baseline Array (VLBA). Identifying statistically significant samples of dual AGNs with pair separations < 1 kpc is also challenging. Since large scale surveys, such as the Sloan Digital Sky Survey (SDSS), are seeing-limited, there is no way to systematically identify mergers with close nuclear separations (< 1 kpc)

through resolved imaging, even in the nearby universe. For these reasons, the dual AGN population remains statistically unconstrained for spatial separations < 1 kpc. There have been attempts to utilize large scale optical surveys such as SDSS to pre-select for dual AGN systems. Detections of double-peaked [O III] $\lambda 5007$ emission in SDSS fibers have been considered as a possible signature of the orbital motion of kpc-scale dual SMBH systems (e.g. Wang et al. 2009; Liu et al. 2010b; Smith et al. 2010; Lyu & Liu 2016; Comerford et al. 2018; Kim et al. 2020; Maschmann et al. 2020). However, several high spatial resolution follow-up studies on targets selected with this method have resulted in a small percentage ($\sim 2\%$) of targets containing dual AGNs (e.g. Liu et al. 2010a; Comerford et al. 2011; Fu et al. 2011a,b; Comerford et al. 2013; Liu et al. 2013; Comerford et al. 2015; Müller-Sánchez et al. 2015). In many targets these double-peaked emission lines have been observed to be produced through other mechanisms such as bi-conical outflows from a single narrow line region or rotating disks, demonstrating that this technique is ineffective at finding closely separated dual AGNs (e.g. Rosario et al. 2010; Fu et al. 2012; Shen et al. 2013; McGurk et al. 2015).

In recent years, a novel technique has emerged that utilizes Gaia’s high-precision astrometry to identify potential sub-kpc dual AGNs through “varstrometry”, the detection of variability induced astrometric “jitter”, i.e., temporal shifts in the photocenter of unresolved sources. Sources with significant astrometric jitter can potentially be the indirect signatures of dual AGNs (e.g. Shen et al. 2019; Hwang et al. 2020; Chen et al. 2022, 2023b; Wang et al. 2023; Schwartzman et al. 2024; Uppal et al. 2024). However, follow-up observations of astrometrically-variable sources using high-resolution optical and radio imaging have yielded few new confirmed dual AGNs. A key limitation of the varstrometry method is that it requires at least one optically obscured AGN in order to enable detection with Gaia. This presents a challenge, as enhanced AGN obscuration is theoretically predicted (Hopkins & Hernquist 2006; Snyder et al. 2013; Blecha et al. 2018) and commonly observed in late-stage mergers (Satyapal et al. 2014; Ricci et al. 2017). Additionally, the detectability of the astrometric signal depends sensitively on a combination of parameters such as projected separation, flux ratio, and amplitude of variability. A more reliable systematic pre-selection strategy that exploits large area sky surveys in the infrared is needed to expand the number of dual AGNs at close pair separations in the nearby universe and characterize their properties.

In this work, we explore a new method to pre-select dual AGNs using mid-infrared surveys. By exploiting the all-sky nature of the Wide-field Infrared Survey Explorer (WISE; Wright et al. 2010) and its sub-arcsecond astrometric precision, we identified a large population of nearby ($z < 0.291$) advanced mergers with mid-infrared

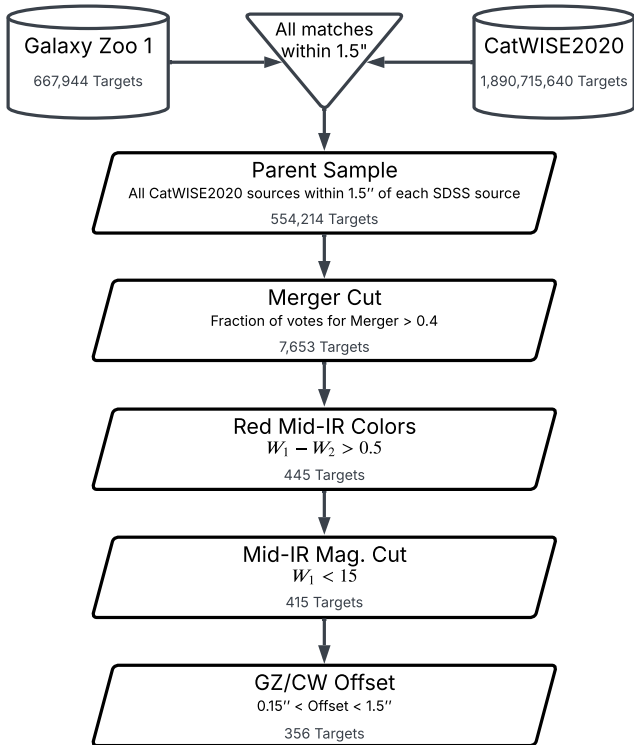


Figure 1. Selection steps for sample of 356 galaxy merger systems with red WISE colors and significant SDSS/WISE offsets ($0.15'' < \text{offset} < 1.5''$).

(MIR) colors indicative of AGNs and significant offsets between their infrared and optical nuclear coordinates as measured by SDSS and WISE. Although the spatial resolution of both WISE and SDSS is insufficient to resolve nuclei separated by less than $\sim 1.5''$ in late-stage mergers, the astrometric precision of both surveys can reveal positional offsets between the optical and infrared centroids on sub-arcsecond scales. Offsets between the WISE and SDSS coordinates in the sample of mergers can therefore be used as a systematic way to find previously unresolved sub-structure in large samples of galaxies in which multiple AGNs may reside. Note that MIR AGN color selection alone guarantees the presence of at least one AGN, and is known to be an effective pre-selection technique in finding dual AGNs in mergers (Satyapal et al. 2017; Blecha et al. 2018; Pfeifle et al. 2019a,b). Our combination of MIR color selection and detection of infrared and optical positional offsets in mergers provides a systematic method to pre-select advanced mergers with accretion activity and unresolved substructure possibly revealing closely separated nuclei in which multiple AGNs may reside. We hereafter refer to these positional discrepancies between SDSS and CatWISE2020 as SDSS/WISE offsets.

A large scale study of mergers with closely separated nuclei in local galaxies is a crucial step in gaining insight into the growth and evolution of SMBHs and their

impact on their host galaxies. Recent JWST observations are uncovering populations of dual and possibly triple AGNs at high redshifts that are spatially resolved (Perna et al. 2023; Li et al. 2024), and signatures of possible dual broad lines in single aperture spectra suggestive of dual AGN on 100 pc scales (Maiolino et al. 2023). However, these dual AGN candidates may turn out to be double-peaked emitters, which can exhibit a vast variety of line profiles and structures (Ward et al. 2024). These observations are suggesting dual AGN fractions of 20-30% (Perna et al. 2023), significantly higher than that found in the local universe (Liu et al. 2011; Koss et al. 2012; De Rosa et al. 2018), and possibly an order of magnitude higher than predicted by some simulations (Volonteri et al. 2022; Chen et al. 2023a). These studies emphasize the critical role that galaxy mergers play in SMBH growth and galaxy evolution during earlier cosmic epochs. While JWST is uncovering this new population, the sensitivity and spatial resolution necessary to carry out a detailed spatially resolved study of AGN pairs with $\lesssim 1$ kpc is still only possible at low redshift.

The goal of this work is to explore a pre-selection strategy that can identify a sample of late-stage mergers harboring likely AGNs with unresolved secondary emission in which nuclei may reside. The resulting sample may provide a pathway for a large sample of mergers to be identified with closely separated nuclei in a largely unexplored regime of parameter space. We present a Keck Near Infrared Camera 2 (NIRC2) imaging study of a sample of 48 late stage mergers selected with our SDSS/WISE positional offset method in which we assess how well this method detects and traces substructure left unresolved by SDSS or WISE. In Section 2 we present the sample selection for this study and expand upon the SDSS/WISE offset selection method. We present the NIRC2 observations and data reduction in Section 3. We detail the results of our analysis of the NIRC2 images and discuss the success and failures of the offset selection method in Section 4. Finally in Section 5 we provide our conclusions from this study. We note that the use of “offset” in this work refers to the SDSS/WISE positional offset and is not the same term as “offset AGN”, which refers to single AGNs located off-nucleus in galaxy mergers. To calculate distances, we assume a Λ CDM cosmology with $H_0 = 70 \text{ km s}^{-1} \text{ Mpc}^{-1}$, and $\Omega_M = 0.3$, and $\Omega_\Lambda = 0.7$.

2. SAMPLE SELECTION

2.1. Keck Merger Sample

We have developed a pre-selection method for detecting candidate dual AGNs from Galaxy Zoo (Lintott et al. 2008) and CatWISE2020 (Marocco et al. 2021) detections. We selected all matches within a $1.5''$ radius between the full Galaxy Zoo DR1 table and the CatWISE2020 catalog, where Galaxy Zoo positions are derived from SDSS DR7. This resulted in 554,214 matches corresponding to 549,279 Galaxy Zoo targets. We then

Archival NIRC2 Observations

SDSS Name	NIRC2 Camera	Filter	Date Observed	Program ID	Program PI	Ref.
J111519.98+542316.7	Wide	K_p	2013-06-17	H230N2L	Koss	N/A
J114642.47+511029.6	Wide	K_p	2010-06-04	C304N2L	Djorgovski	Fu et al. (2011a)
J123915.40+531414.6	Wide	K_p	2010-06-04	C304N2L	Djorgovski	Fu et al. (2011a)
J124046.40+273353.6	Wide	K_p	2013-01-24	H208N2L	Koss	N/A
J131517.26+442425.5	Wide	K_p	2022-05-13	Y076	Urry	N/A
J131535.06+620728.6	Wide	K_s	2017-04-06	Z229	Ryder	N/A
J132035.40+340821.5	Wide	K_s	2017-04-06	Z229	Ryder	N/A
J134442.16+555313.5	Narrow	K_p	2012-05-20	U063N2L	Max	U et al. (2013)
J135429.05+132757.2	Wide	K_p	2013-06-17	H230N2L	Koss	N/A
J135646.10+102609.0	Wide	K_p	2010-06-03	C304N2L	Djorgovski	Fu et al. (2011a)
J163115.52+235257.5	Wide	K_p	2013-06-16	H230N2L	Koss	N/A

Table 1. List of targets with archival NIRC2 imaging data included in the Keck merger sample.

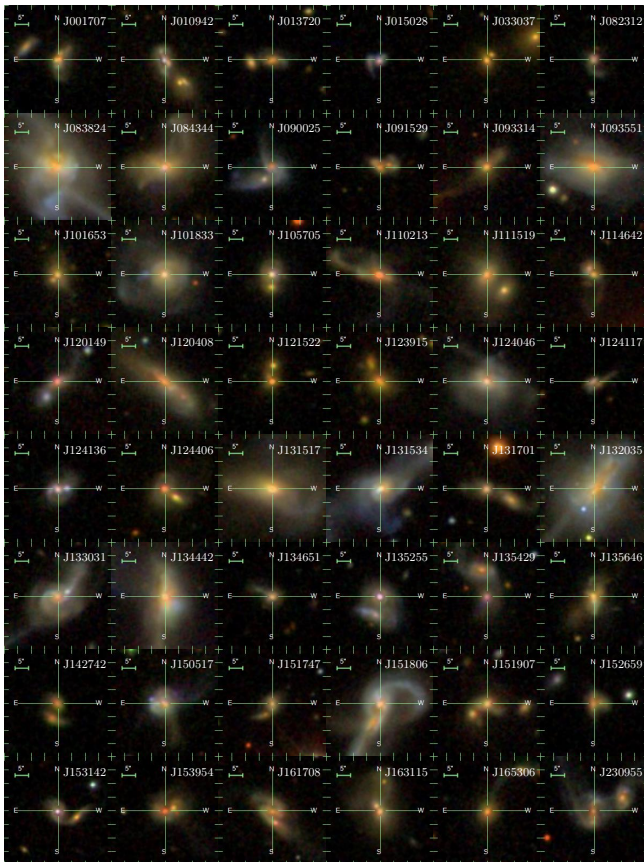


Figure 2. SDSS cutout images of our sample of mergers containing SDSS/WISE offsets between $0.15''$ and $1.5''$. Each cutout has dimensions of $40'' \times 40''$.

selected galaxies that have a high likelihood of being strongly disturbed mergers based on the Galaxy Zoo’s weighted merger-vote fraction parameter, f_m , where $f_m > 0.4$ indicates a system is a strong merger candidate (Darg et al. 2010). We also applied a MIR color cut of $W_1 - W_2 > 0.5$ which has been shown to be an

BPT Diagram of Keck Merger Sample

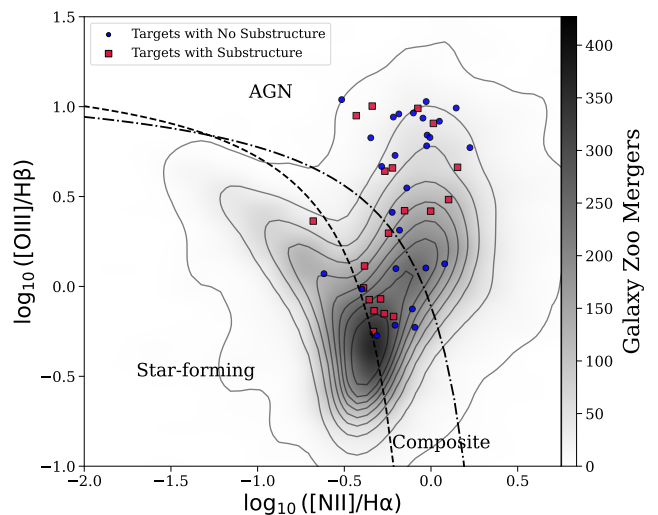


Figure 3. BPT diagram of the 48 target Keck merger sample (SDSS/WISE offset $< 1.5''$) and the parent sample of mergers in Galaxy Zoo. The narrow emission line ratios were drawn from the MPA-JHU DR8 Catalog (Kauffmann et al. 2003a; Brinchmann et al. 2004; Tremonti et al. 2004). Crimson squares correspond to systems with substructure (see Section 4.1) and blue points correspond to all other galaxies in our sample. The shaded contours correspond to all merger systems ($f_m > 0.4$) in Galaxy Zoo. The dashed line shows the empirical “pure star formation” demarcation from Kauffmann et al. 2003b and the dashdotted line shows the theoretical “maximum starburst line” from Kewley et al. 2001; “composite” galaxies fall between the two. Note that one target (J033037) is not included in this plot due to it having a signal-to-noise ratio < 5 in the relevant emission lines.

extremely reliable selection criterion to identify AGN activity in mergers (Blecha et al. 2018). To ensure ro-

Color-Color Diagram of Keck Merger Sample

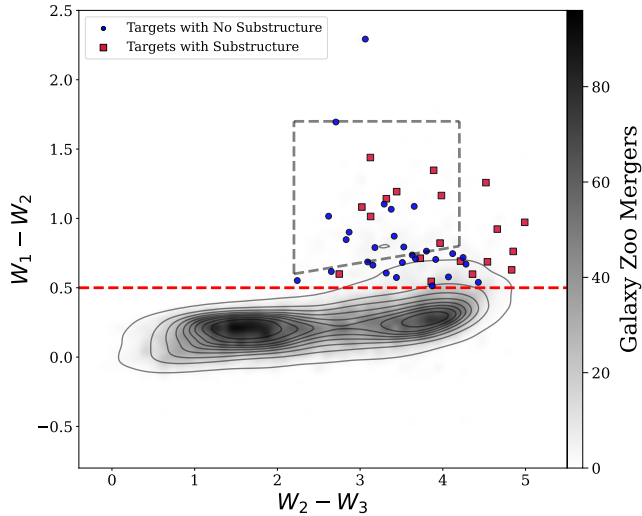


Figure 4. A WISE color-color plot of the 48 target Keck merger sample and the parent sample of mergers in Galaxy Zoo. Crimson squares correspond to systems in our sample with substructure (see Section 4.1) and blue points correspond to all other galaxies in our sample. The shaded contours correspond to all merger systems ($f_m > 0.4$) in Galaxy Zoo. The red dotted horizontal line illustrates the $W_1 - W_2 > 0.5$ color cut applied to the sample (Blecha et al. 2018). The dashed grey box corresponds to the stringent AGN wedge defined in Jarrett et al. 2011. Note that one target (J152659) from the merger sample is not included in this plot since it does not have an available W_3 magnitude.

bust detections in CatWISE2020, we apply a magnitude cut of $W_1 < 15$ where the reliability of a CatWISE2020 detection is above $\sim 98\%$ (Marocco et al. 2021).

This selection criteria resulted in 415 matches across 413 highly disturbed merger systems with red WISE colors, ensuring that we are selecting from the most likely targets to harbor at least one AGN (e.g. Blecha et al. 2018). We then leverage the high astrometric precision of CatWISE2020 and SDSS, with astrometric accuracies of 50 mas and 150 mas respectively, to select sources with significant positional offsets between CatWISE2020 and SDSS ($0.15'' < \text{offset} < 1.5''$). We define the lower and upper limits of the acceptable range of offsets as the astrometric precision of SDSS, 150 mas, and the approximate spatial resolution limit of SDSS. Since both SDSS and CatWISE2020 can measure the position of a galaxy’s nucleus with great precision, a discrepancy between these measurements may be indicative of unresolved nuclear substructure such as bright star clusters, multiple nuclei or AGN. In Galaxy Zoo, for targets with more than one matching CatWISE2020 coordinate, we expect to find more than one unresolved source of emission traced by each CatWISE2020 coordinate. Since the

$E_{(B-V)}$ Distribution of Keck Merger Sample

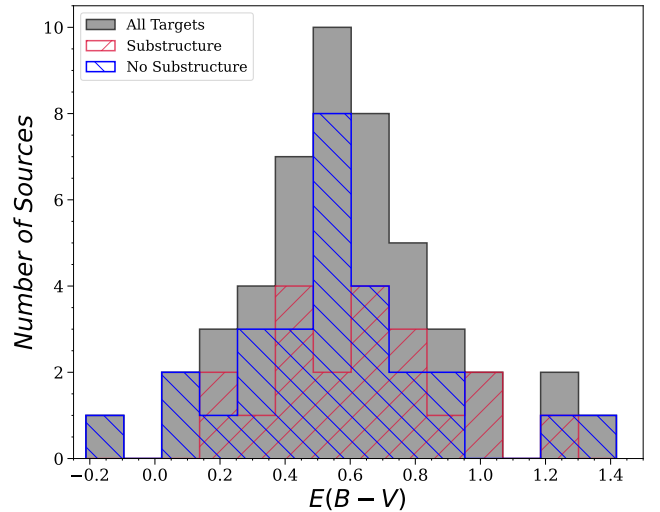


Figure 5. A histogram showing the distribution of extinctions in the Keck merger sample. The extinction coefficient, $E_{(B-V)}$, is calculated from the MPA-JHU DR8 Catalog (Kauffmann et al. 2003a; Brinchmann et al. 2004; Tremonti et al. 2004). The grey bins corresponds to all targets in our sample, the blue hatched bins to the targets with no substructure and the crimson hatched bins to the targets with substructure. (see Section 4.1).

target selection in our methodology begins with mergers classified as AGNs based on their WISE MIR colors, we optimize the chance of revealing at least one or more AGN with higher resolution follow-up observations.

The SDSS/WISE offset criterion results in a parent sample of 356 merger systems with red mid-IR colors and one or more SDSS/WISE offsets. Our target selection methodology is summarized in Figure 1. We then selected 37 targets with nearby guide stars for follow-up high resolution Adaptive Optics (AO) NIRC2 imaging at the Keck observatory. We also included 11 targets with publicly available NIRC2 imaging in the Keck archive (see Table 1), resulting in a sample of 48 galaxy mergers with Keck AO imaging (see Table 2). With this imaging data we search for evidence of previously unresolved substructure and/or closely separated nuclei in these late-stage mergers.

Galaxies in our sample are classified as AGNs or star-forming (SF) galaxies based on their optical narrow emission line ratios, using the Baldwin-Philips-Terlevich diagram (BPT; Baldwin et al. 1981). Classifications follow the criteria of Kauffmann et al. (2003b, K_{03}), Kewley et al. (2001, K_{01}), and Stasińska et al. (2006, S_{06}) applied to emission line fluxes from the MPA-JHU DR8 Catalog (Kauffmann et al. 2003a; Brinchmann et al. 2004; Tremonti et al. 2004). Only spectra with signal-to-noise ratios greater than 5 in the relevant narrow lines

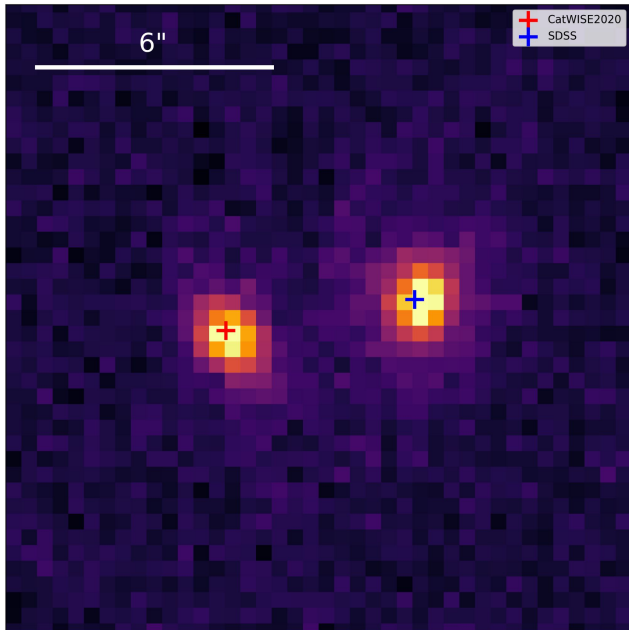


Figure 6. Example UKIDSS K band cutout image of J131012.68+001809.3, one of the targets included in the expanded UKIDSS sample. We overlay the offset SDSS and WISE coordinates for this system demonstrating how the SDSS/WISE offset traces a merger system unresolved by WISE.

are classified with the BPT diagram. We also use the three-band AGN color cut from Jarrett et al. (2011) to identify MIR AGNs in the sample.

The target sample is made up of local galaxies, with a median redshift of 0.105. We show SDSS cutout images of the host galaxies of this sample in Figure 2. In Figure 3 we show the optical narrow line ratios of the sample on the BPT diagram, with 30 targets in the AGN region, 15 in the composite region, and 2 in the star forming region. Note that one target was not included in the BPT diagram due to it having a signal-to-noise ratio < 5 in one of the relevant emission lines. In Figure 4 we plot the WISE colors of this sample ($W_1 - W_2$ vs. $W_2 - W_3$), with 19 targets falling within the stringent AGN wedge defined in Jarrett et al. 2011. In Figures 3 and 4, we include the optical narrow line ratios and mid-IR colors of the general population of galaxies in Galaxy Zoo deemed to be highly disturbed mergers ($f_m > 0.4$; Darg et al. 2010) as background contours. It is clear that a much greater fraction of the target sample has line ratios concentrated in the AGN or composite region (95.8%) than the general merger population in Galaxy Zoo (58.8%). Similarly in Figure 4, a much greater fraction of the target sample lies within the AGN wedge (40%) than the fraction of the general galaxy merger population (1.92%), as expected by design given the mid-IR selection criteria of the sample. Based on these optical and infrared emission properties,

it is clear that a higher fraction of this sample is likely to contain one or more AGN than the general population of galaxy mergers. Additionally, we show the distribution of extinctions for this sample in Figure 5.

A crossmatch with The Big Multi-AGN Catalog (The Big MAC; Pfeifle et al. 2024) reveals that the 48 target Keck merger sample (SDSS/WISE offset $< 1.5''$) contains 13 previously identified candidate dual AGN and 3 confirmed dual AGN. However, only two of the three confirmed dual AGN have separations small enough to correspond to the SDSS/WISE offsets we detect, the rest of the systems are too widely separated to be attributable to an SDSS/WISE offset smaller than $1.5''$. The candidate/confirmed dual AGNs with very large separations are resolved galaxy pair systems with an SDSS/WISE offset corresponding to substructure in one of the galaxies in the dual system. These mergers may potentially contain more than two AGNs.

2.2. Supplementary Expanded UKIDSS Sample

Because the field of view of our NIRC2 images is too small to include any nearby stars, it is not possible to obtain an accurate World Coordinate System (WCS) solution mapping array pixels to sky positions for the Keck data. In order to explore the reliability of our methodology and its dependence on offset, we expanded our sample to include a wider range of offsets, $0.15'' - 6''$ (the spatial resolution of WISE), resulting in 540 merger systems that are resolvable with UKIRT InfraRed Deep Sky Surveys (UKIDSS; Lawrence et al. 2007), where the WCS coordinates can be used to determine if any sources revealed in the near-infrared (NIR) images correspond to either the SDSS or WISE coordinates. From this sample, we selected 3 additional targets to include in our Keck imaging program, identified 2 more targets with archival NIRC2 imaging, and found 61 more targets with SDSS/WISE offsets between $0.8''$ (\sim the spatial resolution of UKIDSS) and $6''$ with UKIDSS cutout imaging. Note that this expanded sample includes all targets from the previously defined 48 target Keck merger sample, and thus contains 114 merger systems with Keck or UKIDSS imaging. For the UKIDSS targets in this sample, we are able to overlay the SDSS and WISE coordinates on the UKIDSS images and compare these coordinates with the emission revealed in the near-infrared UKIDSS images (see Figure 6).

2.3. Comparison Samples

Our goal in this work is to determine if our adopted pre-selection strategy, searching for advanced red mergers with significant SDSS/WISE offsets, is successful in identifying unresolved substructure in which one or more AGNs may reside. Unfortunately, archival NIRC2 data is limited, preventing a large statistical analysis. Nonetheless, we constructed two comparison samples to assess whether our success in detecting substructure is enhanced by the SDSS/WISE offset selection or if

General Properties of Keck Merger Sample

SDSS Name	Name	R.A.	Dec	$W_1 - W_2$	Offset	z	E_{B-V}	Optical Classification
J001707.95+011506.3	...	4.283	1.252	1.014	0.511	0.106	1.021	K_{01}
J010942.21-004417.4	...	17.426	-0.738	0.713	0.443	0.089	0.486	K_{03}
J013720.02+005722.2	...	24.333	0.956	0.514	0.280	0.198	0.832	K_{03}
J015028.40+130858.4	...	27.618	13.150	1.258	0.275	0.147	0.299	S_{06}
J033037.40-003304.0	...	52.656	-0.551	0.552	0.169	0.147	0.470	N/A
J082312.61+275139.8	...	125.803	27.861	0.972	0.294	0.168	0.659	K_{03}
J083824.00+254516.3	NGC 2623	129.600	25.755	0.718	0.912	0.018	1.190	K_{01}
J084344.98+354942.0	...	130.937	35.828	0.709	0.387	0.0540	0.438	K_{01}
J090025.37+390353.7	...	135.106	39.065	2.293	0.510	0.058	0.858	K_{03}
J091529.62+090601.5	...	138.873	9.100	1.439	0.431	0.143	0.662	K_{01}
J093314.80+630945.0	...	143.312	63.163	0.822	0.167	0.118	0.564	K_{01}
J093551.60+612111.3	UGC 5101	143.965	61.353	1.695	0.318	0.040	1.418	K_{01}
J101653.82+002857.0	...	154.224	0.483	1.082	0.275	0.116	0.1849	K_{01}
J101833.64+361326.6	...	154.640	36.224	0.663	0.189	0.054	0.496	K_{01}
J105705.40+580437.4	VII Zw 353	164.273	58.077	0.606	0.308	0.140	0.064	K_{03}
J110213.01+645924.8	...	165.554	64.990	1.193	0.276	0.078	0.742	K_{01}
J111519.98+542316.7	...	168.833	54.388	0.790	0.294	0.070	0.671	K_{01}
J114642.47+511029.6	...	176.677	51.175	0.670	0.810	0.130	0.189	K_{01}
J120149.75-015327.5	...	180.457	-1.891	0.574	0.316	0.091	0.499	K_{01}
J120408.82+132117.0	UGC 7043	181.037	13.355	0.546	0.486	0.076	0.744	K_{01}
J121522.77+414620.9	...	183.845	41.773	0.901	0.321	0.196	0.271	K_{01}
J123915.40+531414.6	...	189.814	53.237	0.599	0.306	0.202	0.396	K_{01}
J124046.40+273353.6	...	190.193	27.565	1.103	0.315	0.057	0.889	K_{03}
J124117.64+273252.3	...	190.324	27.548	0.598	0.411	0.140	0.685	K_{03}
J124136.22+614043.4	...	190.401	61.679	0.746	0.259	0.135	0.538	K_{01}
J124406.61+652925.2	...	191.028	65.490	0.794	0.537	0.107	0.612	K_{01}
J131517.26+442425.5	UGC 8327	198.822	44.407	1.142	0.689	0.036	0.580	K_{03}
J131535.06+620728.6	UGC 8335B	198.896	62.125	0.762	0.585	0.031	0.659	K_{03}
J131701.41+004509.7	...	199.256	0.753	0.682	0.187	0.138	0.479	K_{01}
J132035.40+340821.5	IC 883	200.148	34.139	0.687	1.209	0.023	1.265	K_{03}
J133032.00-003613.5	VIII Zw 318	202.634	-0.604	0.578	0.300	0.054	0.585	K_{01}
J134442.16+555313.5	MRK 273	206.176	55.887	1.165	0.799	0.037	1.031	K_{01}
J134651.82+371231.0	...	206.716	37.209	0.692	0.230	0.215	0.440	K_{01}
J135255.67+252859.6	...	208.232	25.483	0.686	0.198	0.064	0.276	SF*
J135429.05+132757.2	...	208.621	13.466	1.016	0.184	0.063	0.117	K_{01}
J135646.10+102609.0	...	209.192	10.436	1.347	0.258	0.123	0.213	K_{01}
J142742.68+050318.4	...	216.928	5.055	0.764	0.400	0.159	0.571	K_{01}
J150517.88+080912.7	...	226.325	8.154	0.923	0.194	0.039	0.779	K_{03}
J151747.47+334740.4	...	229.448	33.795	0.704	0.494	0.119	0.493	K_{01}
J151806.13+424445.0	VV 705	229.526	42.746	0.629	0.500	0.040	0.891	K_{03}

Table 2. Source information for our 48 target Keck merger sample drawn from SDSS, catWISE2020, and the MPA JHU Catalog. Column 1: SDSS source name. Column 2 & 3: SDSS right ascension (RA) and declination (Dec) source coordinates in degrees. Column 4: WISE $W_1 - W_2$ color. Column 5: SDSS/WISE positional offset. Column 6: Redshift. Column 7: E_{B-V} value derived from the MPA-JHU catalog. Column 8: Optical BPT classification from three different division schemes (K_{01} : Kewley et al. 2001, K_{03} : Kauffmann et al. 2003b, S_{06} : Stasińska et al. 2006).

Name	SDSS Name	R.A.	Dec	$W_1 - W_2$	Offset	z	E_{B-V}	Optical Classification
J151907.33+520606.0	...	229.781	52.102	1.066	0.332	0.138	0.705	K_{01}
J152659.44+355837.0	...	231.748	35.977	1.437	0.376	0.055	0.452	K_{03}
J153142.10+051801.6	...	232.925	5.300	0.617	0.232	0.123	N/A	K_{03}
J153954.78+272758.7	...	234.978	27.466	0.847	0.267	0.119	0.723	K_{01}
J161708.95+222627.9	...	244.287	22.441	0.872	0.672	0.066	0.484	K_{01}
J163115.52+235257.5	...	247.815	23.883	0.736	0.168	0.059	0.521	K_{01}
J165306.55+262638.0	...	253.277	26.444	1.087	0.261	0.119	0.340	K_{01}
J230955.10+002148.8	...	347.480	0.364	0.539	0.641	0.104	0.492	K_{03}

Table 2. (Continued) Source information for our 48 target Keck merger sample drawn from SDSS, catWISE2020, and the MPA JHU Catalog. Column 1: SDSS source name. Column 2 & 3: SDSS right ascension (RA) and declination (Dec) source coordinates in degrees. Column 4: WISE $W_1 - W_2$ color. Column 5: SDSS/WISE positional offset. Column 6: Redshift. Column 7: E_{B-V} value derived from the MPA-JHU catalog. Column 8: Optical BPT classification from three different division schemes (K_{01} : Kewley et al. 2001, K_{03} : Kauffmann et al. 2003b, S_{06} : Stasińska et al. 2006).

BPT Diagram of Keck Non-merger Sample

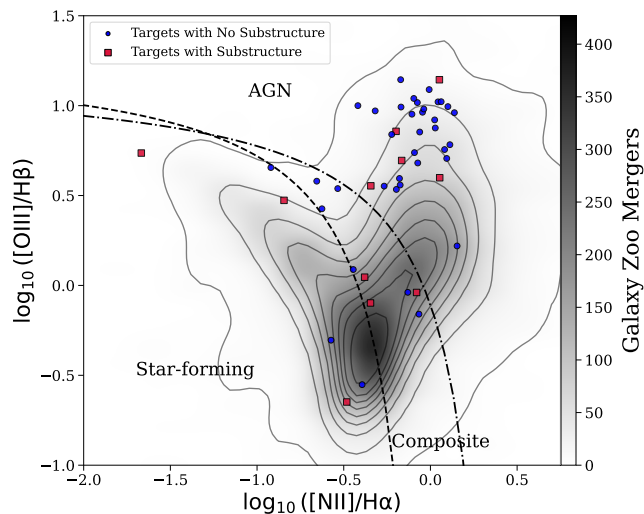


Figure 7. Same as Figure 3 except the foreground data corresponds to the non-merger comparison sample.

it is primarily due to the fact we are selecting late-stage mergers. First, we constructed a sample of isolated galaxies from Galaxy Zoo, with no evidence of an ongoing merger, that also have an SDSS/WISE offset. To generate this sample we applied the same selection method detailed in Section 2.1, but replaced the merger selection criteria with a selection for galaxies with low likelihood of being a merger ($f_m < 0.4$). This resulted in a sample of 5,815 non-merger systems with red WISE colors ($W_1 - W_2 > 0.5$) that meet our magnitude cut, $W_1 < 15$, and significant SDSS/WISE offsets ($0.1'' < \text{Offset} < 1.5''$). From this sample there are 48 targets with archival NIRC2 imaging data, comprising our non-merger comparison sample. In Figures 7, 8, and 9 we show the optical narrow line ratios on the BPT diagram,

Color-Color Diagram of Keck Non-merger Sample

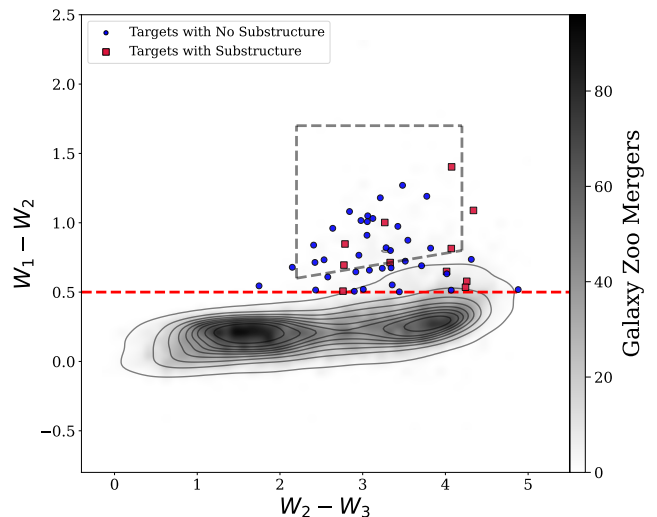


Figure 8. Same as Figure 4 except the foreground data corresponds to the non-merger comparison sample.

the WISE colors ($W_1 - W_2$ vs. $W_2 - W_3$) and the distribution of extinctions for this sample.

While the limited availability of archival NIRC2 data precludes the construction of a statistically significant and robust control sample, we compared the redshifts, W_1 magnitudes, WISE colors and SDSS/WISE offsets of the non-merger sample with our merger sample as shown in Figures 10 and 11. Based on a two-sample Kolmogorov-Smirnov test (KS-test) of each distribution, there is no significant difference between the distribution of offsets, redshifts, W_1 magnitude or WISE colors in the merger sample and the non-merger sample.

To further test whether any substructure identified in our Keck merger sample is truly detected by

$E_{(B-V)}$ Distribution of Keck Merger Sample

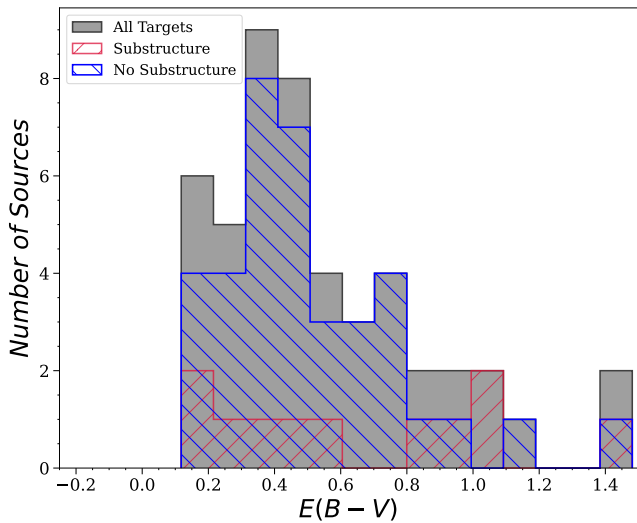


Figure 9. Same as Figure 5 except the displayed data corresponds to that of the non-merger comparison sample.

the SDSS/WISE offset or merger cut, we also generated another comparison sample of mergers with no SDSS/WISE offset. We find that there are 50 merger systems with red WISE colors ($W_1 - W_2 > 0.5$) that meet our magnitude cut, $W1 < 15$, and no significant SDSS/WISE offset ($< 0.15''$). From this sample we identify 11 targets with archival NIRC2 imaging data comprising our non-offset comparison sample. A summary of these samples is listed in Table 3.

3. OBSERVATIONS AND DATA REDUCTION

We observed a total of 40 targets (37 targets from the Keck merger sample and 3 with SDSS/WISE offsets $> 1.5''$ from the expanded Keck/UKIDSS merger sample) with the Keck II Telescope over three nights between 2021 and 2022 (UT 2021 September 19, UT 2022 March 19, and UT 2022 March 20) with the NIRC2 camera (PI: K. Matthews), using Laser and Natural Guide Star Adaptive Optics correction (LGSAO & NGS AO, Wizinowich et al. 2000; van Dam et al. 2006; Wizinowich et al. 2006). For the two observing nights in 2022, images were taken with the Narrow-Field Camera (FOV: $10'' \times 10''$, pixel scale: $0.009942'' \text{pixel}^{-1}$) in the K_p filter ($\lambda_c = 2.124 \mu\text{m}$, $\Delta\lambda = 0.351 \mu\text{m}$) with a consistent exposure time of $3 \times 300\text{s}$ applied to each target. Both nights were photometric, with a natural seeing that ranged from $0.6''$ to $1.0''$. For the observing night in 2021, images were taken with the Wide-Field Camera (FOV: $40'' \times 40''$, pixel scale: $0.039686'' \text{pixel}^{-1}$) for 8 targets and with the Narrow-Field Camera for one target (J015028). All images were taken in the K_p filter under photometric conditions, with a natural seeing of $0.5''$; exposure times ranged from $6 \times 180\text{s}$ to $9 \times 180\text{s}$ for the

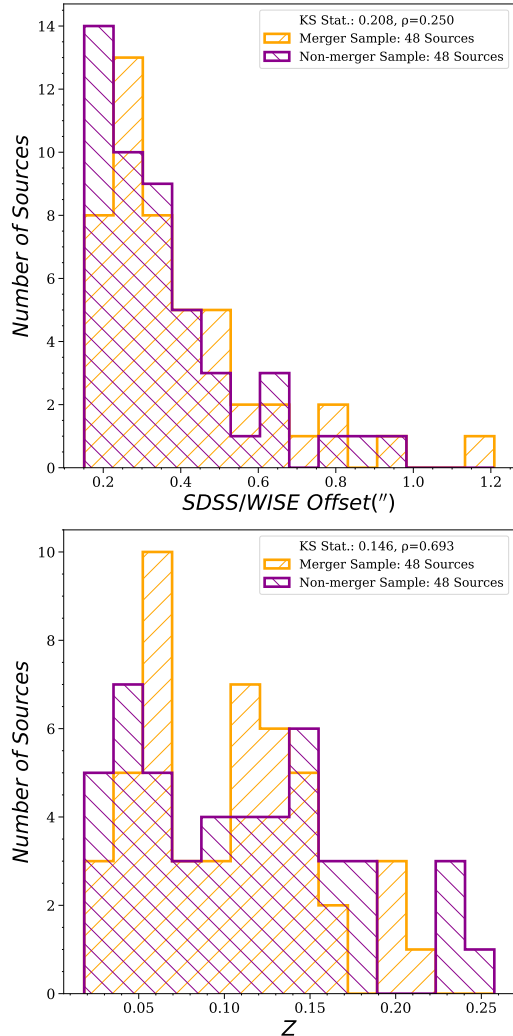


Figure 10. Histograms comparing the distributions of SDSS/WISE offset and redshift of the 48 target merger sample and 48 target non-merger sample. We conduct a two-sample KS-test for each variable and include the results in the legend of each histogram.

Wide-Field Camera images and $5 \times 300\text{s}$ for the Narrow-Field Camera image. A 3-point dither pattern strategy was employed for all observations across all three nights, avoiding a known artifact in the bottom left corner of the image. Additionally, for each science target we obtained corresponding observations of a tip-tilt star to track the system performance. Flat and dark frames were taken on each night for data calibration and standard stars were observed on each night for flux calibration.

The NIRC2 images were reduced using the standard data reduction procedures of dark subtraction, flat-field correction, sky subtraction, bad pixel correction, and correction for geometric distortion. Sky subtraction was performed by subtracting each image by a source free region in another image in the same dither set. Prior to av-

Summary of Samples

	Imaging Type	Selection Criteria	Sample Size	Fraction with Substructure*
Keck Merger Sample	Keck AO	$f_m > 0.4$ $0.15'' < \text{offset} < 1.5''$	48	20 (42%)
Expanded Keck/ UKIDSS Merger Sample	Keck/ UKIDSS	$f_m > 0.4$ $0.15'' < \text{offset} < 6''$ (Keck) $0.8'' < \text{offset} < 6''$ (UKIDSS)	114	71 (62%)
Keck Non-merger Sample	Keck AO	$f_m < 0.4$ $0.15'' < \text{offset} < 1.5''$	48	11 (23%)
Keck Non-offset Sample	Keck AO	$f_m > 0.4$ $\text{offset} < 0.15''$	11	1 (9%)

Table 3. Summary of samples presented in this paper. For each sample we include the type of imaging data utilized, selection criteria, sample size and fraction of the sample that contains substructure. Note: All four samples are selected to have $W_1 < 15$ and $W_1 - W_2 > 0.5$. *See Section 4.1 for definition of substructure.

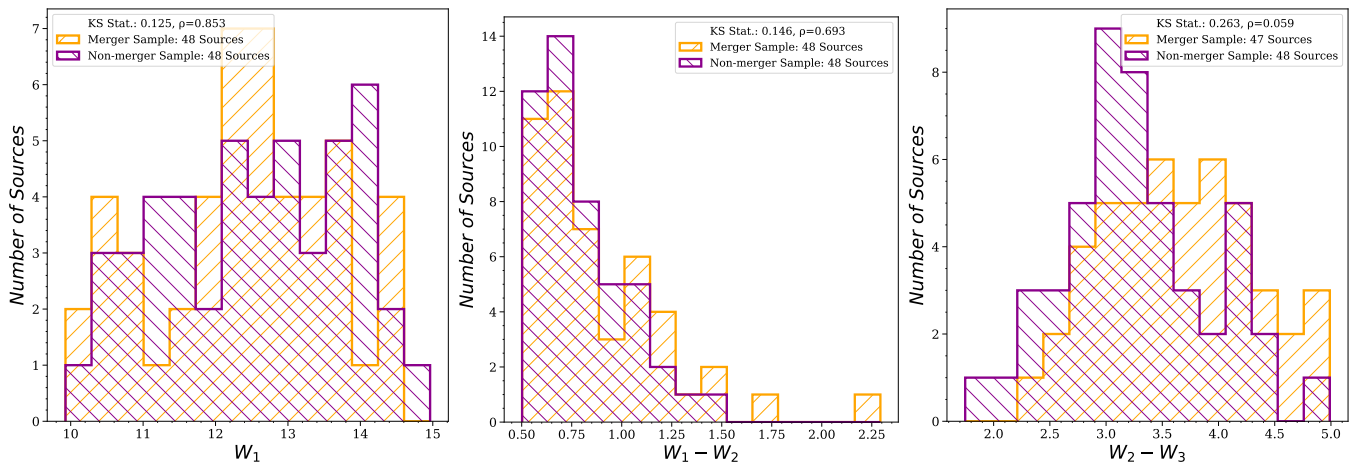


Figure 11. Histograms comparing the distributions of W_1 magnitude, $W_1 - W_2$, and $W_2 - W_3$ of the 48 target Keck merger sample and 48 target Keck non-merger sample. We conduct a two-sample KS-test for each variable and include the results in the legend of each histogram. Note that one target (J152659) from the merger sample is not included in the $W_2 - W_3$ comparison since it does not have an available W_3 magnitude.

eraging images from the three dither positions, each image was individually corrected for geometric distortion using the most up to date Narrow- and Wide-Camera distortion solution (Service et al. 2016) with the IDL script nirc2dewarp.pro.¹ The images were aligned using the centroids of bright nuclear sources prior to averaging. Finally, the images were flux calibrated using the standard stars observed each night. Because the sample consists of advanced mergers with disturbed mor-

phologies and diffuse galaxy light, 2-D surface brightness profile-fitting to extract structural components and identify and extract point-source magnitudes was unsuccessful. The small field of view further limited the ability to fit the background galaxy light with a Sérsic profile. Therefore, in this work, we visually identified all significant sources of emission within the field of view and performed aperture photometry to obtain a flux and magnitude associated with each identified source. For each target in our sample we set an aperture radius equivalent to 1.25 times the full width half-maximum (FWHM) of the corresponding tip-tilt star; this aperture radius was used for all sources identified in an image. In Table 4

¹ <https://www2.keck.hawaii.edu/inst/nirc2/astrometry/nirc2dewarp.pro> written by Keck observer Brian Cameron

we list the fluxes measured for targets containing substructure in the Keck merger sample. Note that the primary goal of this work was to identify substructure that is unresolved in WISE and SDSS, not to carry out a detailed surface brightness profile analysis and extract fluxes through a PSF-fitting analysis. The fluxes are therefore presented merely to assess whether the individual sources identified are likely consistent with individual nuclei in the merger.

In addition, we identified 13 targets with publicly available and pre-calibrated NIRC2 imaging, 11 of which have SDSS/WISE offsets $< 1.5''$ and 2 with SDSS/WISE offsets between $1.5'' - 6''$ (See Table 3 for a summary of the samples). The pre-calibration of these images involves dark subtraction, flat fielding, correction of bad pixels, and distortion correction using B. Cameron’s IDL routine. We then aligned and average combined the pre-calibrated frames for each observation. Flux calibration is not included in the pre-calibration of these targets, thus we do not include fluxes and magnitudes for the archival targets in our sample.

4. RESULTS

4.1. Substructure Detection Rate

In Figure 12, we show the NIRC2 images of the Keck merger sample (see Appendix A for detailed descriptions of individual targets). The targets with substructure are highlighted in green. As can be seen, many of the mergers show intricate structure unresolved by SDSS with several showing two or more sources of compact emission that are separated by less than $1.5''$. In each image, we select a “substructure-pair” consisting of the primary central nucleus and the brightest secondary source of emission in a target galaxy. Eligible secondary sources of emission are restricted based on the size of the SDSS/WISE offset such that offsets $< 1.5''$ can only correspond to sources in the Keck image unresolved by SDSS and offsets $> 1.5''$ can only correspond to sources that are resolved by SDSS. In Table 4, we list the flux, separation and flux ratio of the substructure pair in each target with a substructure detection. The separation between substructure pairs in the NIRC2 images ranges from $0.19''$ to $1.25''$, corresponding to physical separations of 170 pc to 3.86 kpc. Seven of the 48 mergers show pairs of compact structures separated by $\lesssim 1''$ with flux ratios > 0.5 . While an accurate measurement of the source magnitudes requires a detailed fitting of the surface brightness profile which is impossible to do with the current data (see Section 3), these flux ratios suggest that these compact sources are maybe pairs of galaxy nuclei where AGNs may reside. We note however that flux ratios < 0.5 may also correspond to dual AGNs; indeed one source with a flux ratio of 0.411, J134442 (see Appendix A), is a confirmed dual AGN based on multi-wavelength follow-up as indicated in Pfeifle et al. 2024. Thus targets with sources of secondary emission may correspond to AGNs within significantly less massive nu-

Keck Merger Sample Photometry

Name	Offset "	Sep. "	Sep. kpc	Flux mJy	Ratio
J001707	5.630 ± 1.591	...
...	0.511	0.986	1.910	1.826 ± 0.516	0.324
J010942	0.076 ± 0.0005	...
...	0.443	1.129	1.871	0.052 ± 0.0004	0.678
J015028	0.118 ± 0.052	...
...	0.275	0.234	0.599	0.054 ± 0.026	0.549
J082312	0.115 ± 0.005	...
...	0.294	0.564	1.617	0.014 ± 0.001	0.118
J091529	0.050 ± 0.001	...
...	0.431	0.917	2.300	0.011 ± 0.0003	0.225
J093315	0.060 ± 0.001	...
...	0.167	0.190	0.405	0.045 ± 0.001	0.756
J101653	4.041 ± 0.085	...
...	0.275	0.350	0.737	0.073 ± 0.015	0.180
J110213	0.982 ± 0.020	...
...	0.276	0.357	0.524	0.573 ± 0.012	0.584
J120408	0.063 ± 0.001	...
...	0.486	0.740	1.070	0.059 ± 0.001	0.931
J123915*	0.306	1.161	3.855	...	0.860
J124117	0.018 ± 0.0003	...
...	0.411	0.266	0.655	0.019 ± 0.0003	1.031
J131517*	0.689	0.711	0.503	...	0.310
J131534*	0.585	0.287	0.177	...	0.209
J132035*	1.209	0.784	0.365	...	0.755
J134442*	0.799	1.035	0.767	...	0.411
J134651	0.318 ± 0.002	...
...	0.230	0.633	2.209	0.041 ± 0.0003	0.130
J135646*	0.258	1.253	2.771	...	0.400
J150517	0.309 ± 0.003	...
...	0.194	0.347	0.270	0.079 ± 0.001	0.257
J151806	0.950 ± 0.016	...
...	0.500	1.083	0.863	0.128 ± 0.002	0.135
J152659	0.531 ± 0.048	...
...	0.376	0.631	0.677	0.145 ± 0.013	0.272

Table 4. Photometric measurements for each source of emission in a substructure pair (see Section 4.1) for each substructure target in the Keck merger sample. Column 1: Target name. Column 2: SDSS/WISE offset. Columns 3 & 4: Substructure pair separation in " and kpc. Column 5: K_p flux (mJy) with corresponding errors. Column 6: Flux ratio of substructure pair ($f_{secondary}/f_{primary}$). Note: For targets with photometry, the first row corresponds to the central nucleus and thus we do not list a separation or flux ratio for these sources. For archival targets, we include only one row with the SDSS/WISE offset, separation, and flux ratio of the substructure pair, but no flux data, as these targets are not flux calibrated.

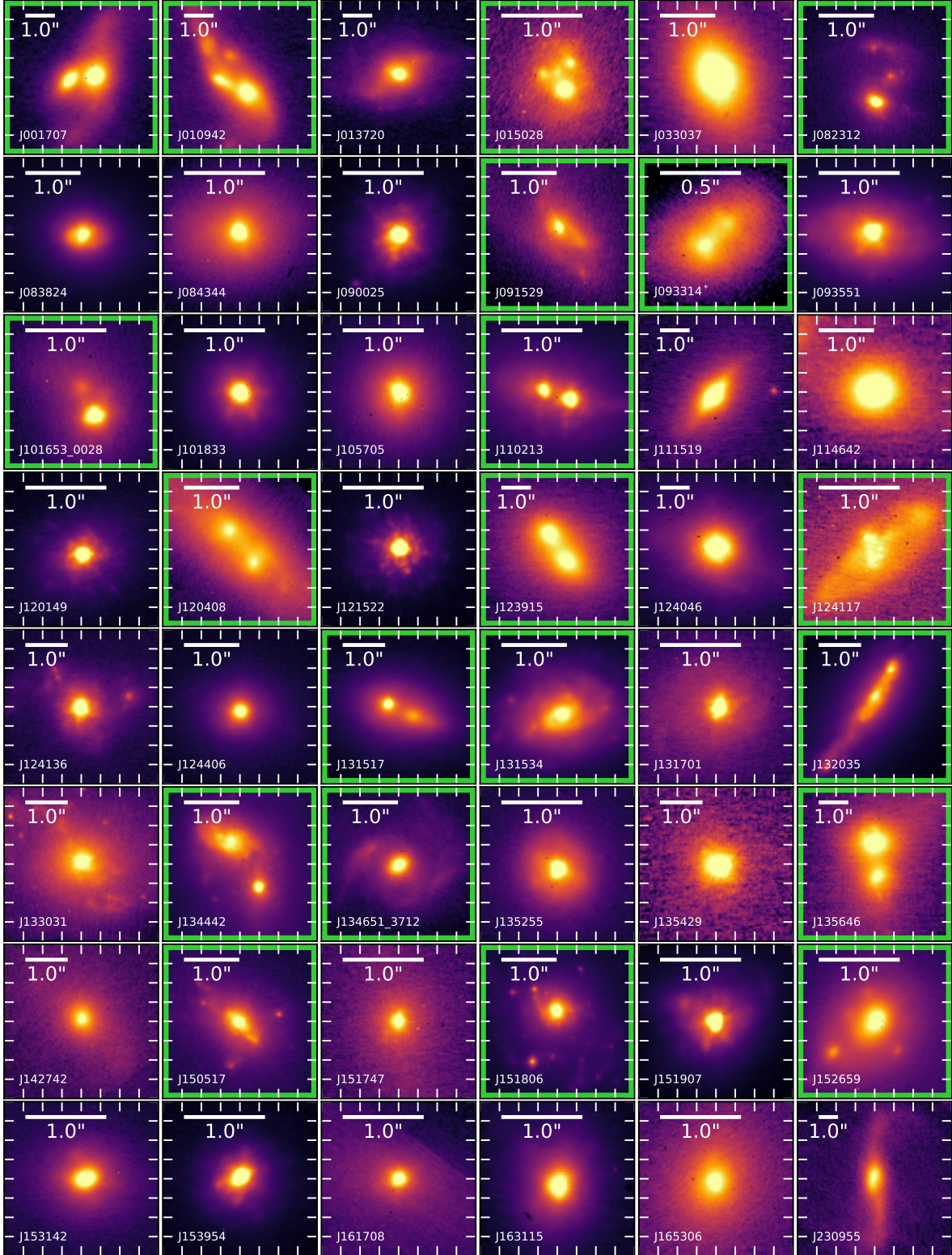


Figure 12. Final NIRC2 AO K_p band cutout images of the 48 target Keck merger sample. North is up and East is to the left in each image. The white scale bar in the top left of each image corresponds to 1 arcsecond. Those targets which we identify as having substructure are highlighted in green (see Appendix A for detailed descriptions).

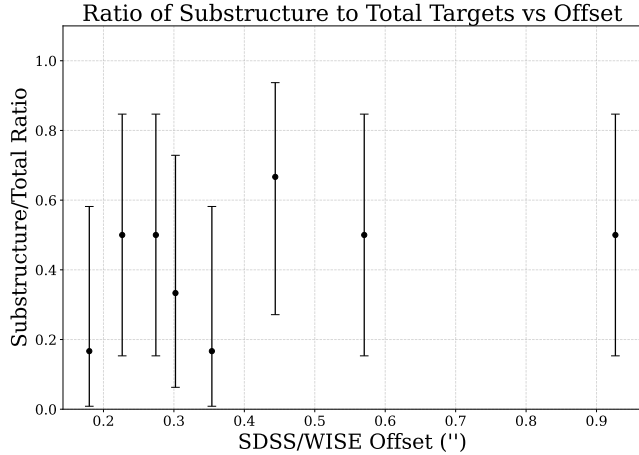


Figure 13. A comparison of substructure detection rate to SDSS/WISE offset in our 48 target Keck merger sample ($0.15'' < \text{offset} < 1.5''$). We define 8 bins that vary in width and position along the X-axis such that the sample size for each bin is relatively the same. For each bin we plot the substructure detection rate for targets with SDSS/WISE offsets within that range. The error bars we include are calculated with binomial statistics, representing a 90% confidence interval.

clei associated with a minor merger. We also note that in some sources, there is significant diffuse and patchy emission that may be the cause of the SDSS/WISE offset. We emphasize that with imaging alone, there is no way to confirm if any of the sources of emission detected are AGNs or star clusters. Furthermore the distinction between a galaxy nuclei and a star cluster is arbitrary.

Our analysis of the reduced and calibrated NIRC2 observations revealed that in the 48 target Keck merger sample (SDSS/WISE offset $< 1.5''$), 20 galaxy mergers contain substructure (41.6%), which we define as significant sources of secondary emission ($f_{\text{secondary}}/f_{\text{primary}} > 0.1$) unresolved by SDSS. Of the targets with substructure, 10 are classified as K_{01} AGN, 9 as K_{03} AGN, and 1 as S_{06} AGN based on their SDSS spectra (see Table 2). In Figures 3 and 4 we show that we detect substructure in 33% of the BPT AGN (10/30), 60% of the composite sources (9/15), 50% of the star-forming sources (1/2) and 42% of the Jarret AGN (8/19) in our sample. Although the number of substructure targets in the AGN and composite regions of Figure 3 is roughly the same, they comprise a larger fraction of the composite targets. Additionally, 73% of the targets with $W_2 - W_3 > 4.2$ have substructure (8/11). In Figure 5 we show the distribution of extinction, as measured by the $E(B-V)$ value from the MPA-JHU catalog, for targets with and without substructure. We find that the detection rate for substructure is significantly higher at larger $E(B-V)$ values, with 52% of targets with $E(B-V)$ values greater than 0.6 containing substructure. In contrast, only 33% of targets with $E(B-V)$ below 0.6 contain

substructure, suggesting that galaxies that display substructure unresolved by SDSS tend to be galaxies with higher extinction. To explore if the detection rate we determine depends on the size of the SDSS/WISE offset, we also calculated the detection rate of substructure in the expanded sample of mergers with offsets between $0.15''$ and $6''$. In the expanded sample of NIRC2 and UKIDSS targets with offsets between $0.15''$ and $6''$ we detect substructure in an additional 51 targets, corresponding to a detection rate of 62% (71/114).

In order to determine the effect of astrometric noise on our detection rate, we calculate the detection rate as a function of offset. In Figure 13 we plot the substructure detection rate in 8 bins, each corresponding to a range of SDSS/WISE offsets. For each bin we take the ratio of total targets within that offset range to the number of those targets in which we detect substructure, i.e. detection rate. Error bars correspond to binomial statistics and represent a 90% confidence interval. There is no clear trend on decreasing success rate with decreasing offset given the error bars, suggesting that the success rate of the selection method is not limited by the astrometric precision of SDSS and WISE for the offsets considered in this work.

4.2. Offset and nuclear pair comparison

To test the validity of the SDSS/WISE offset selection, ideally, the SDSS and WISE coordinates should be overlaid on the images. However, since we cannot spatially register the NIRC2 images, we cannot compare the positions of the sources identified in the Keck images with the SDSS or WISE coordinates. However, we can compare the orientation of the SDSS/WISE offset to the orientation of the substructure detected in the NIRC2 images. In so doing, we can explore whether the structure we are detecting in the Keck images is tracing the offset between the SDSS and WISE coordinates. We conducted this comparison on the 71 targets with substructure in the expanded sample of Keck and UKIDSS mergers with SDSS/WISE offsets spanning the full range between $0.15''$ and $6''$. For each target, we identified a substructure pair (see Section 4.1) and registered its separation and position angle (PA) for comparison with a corresponding SDSS/WISE offset. In the NIRC2 images we cannot determine which of the two coordinates (SDSS or WISE) coincides with the primary nucleus in any given system. Therefore, when registering the PAs of SDSS/WISE offsets, we measure the position angle relative to the SDSS coordinate and then to the WISE coordinate and choose the angle most similar to that of the substructure pair. In the case of the UKIDSS images, the substructure pairs consist of the closest source of emission to the SDSS coordinate and then the source of emission closest to the WISE coordinate and we measure the corresponding separation and PA.

In Figure 14 we compare the angular separations and PAs of the substructure-pairs to the SDSS/WISE offsets for each of the 71 galaxies with substructure. This comparison reveals that the sizes and PAs of the SDSS/WISE offsets are significantly correlated with the separations (Spearman Rank Coefficient: 0.865, ρ : 0.000) and PAs (Spearman Rank Coefficient: 0.871, ρ : 0.000) of the substructure pairs. The PAs of the SDSS/WISE offsets tend to more accurately reflect the orientation of the substructure they detect, whereas the sizes of the SDSS/WISE offsets tend to under-predict the separations of the substructure pairs. This is because the magnitude of the SDSS/WISE offset depends on the relative brightness of the secondary emission source compared to the central nucleus. When both sources have comparable mid-infrared brightness, the WISE centroid shifts toward the midpoint between them. A similar effect occurs for the SDSS centroid in systems with separations smaller than $\sim 1.5''$. The PAs on the other hand do not depend on the relative brightness of the substructure, resulting in a stronger correlation.

4.3. Comparison Sample Results

To better understand the role of the offset and merger cuts in our sample selection, we built a sample of 48 non-mergers ($f_m < 0.4$), with red WISE colors ($W_1 - W_2 > 0.5$), $W_1 < 15$, SDSS/WISE offsets ($0.15'' < \text{offset} < 1.5''$) and NIRC2 imaging (see Section 2.3). In this sample we find that of the 48 targets, 11 have substructure (23%) with 4 targets having flux ratios > 0.5 . When relaxed to offsets up to $6''$, the detection rate is 13 out of 50 targets (26%). Although the non-merger sample contains significantly less targets with substructure than the main sample of mergers, the detection of substructure in non-mergers with SDSS/WISE offsets is still significant. A lack of detections would suggest that the offsets we detect in the merger sample are coincidental and play no role in the detection rate found in the merger sample. However, the 11 detections of substructure in non-mergers suggests that our detection rate cannot be solely due to the merger cut, although it seems the combination of both the offset and merger cut is needed to achieve the detection rate we see in the Keck merger sample. The detection of substructure, especially dual nuclei with flux ratios > 0.5 , in the non-merger sample possibly indicates that we are finding nuclear mergers in systems without morphological indicators of merger activity apparent in SDSS, similar to those found by Koss et al. (2018).

To more robustly test the strength of the offset selection it would be necessary to create another control sample of merger systems which do not have significant offsets between their SDSS and WISE coordinates. We created a sample of 11 NIRC2 imaged merger systems ($f_m < 0.4$), with red WISE colors ($W_1 - W_2 > 0.5$), $W_1 < 15$ and non-significant SDSS/WISE offsets

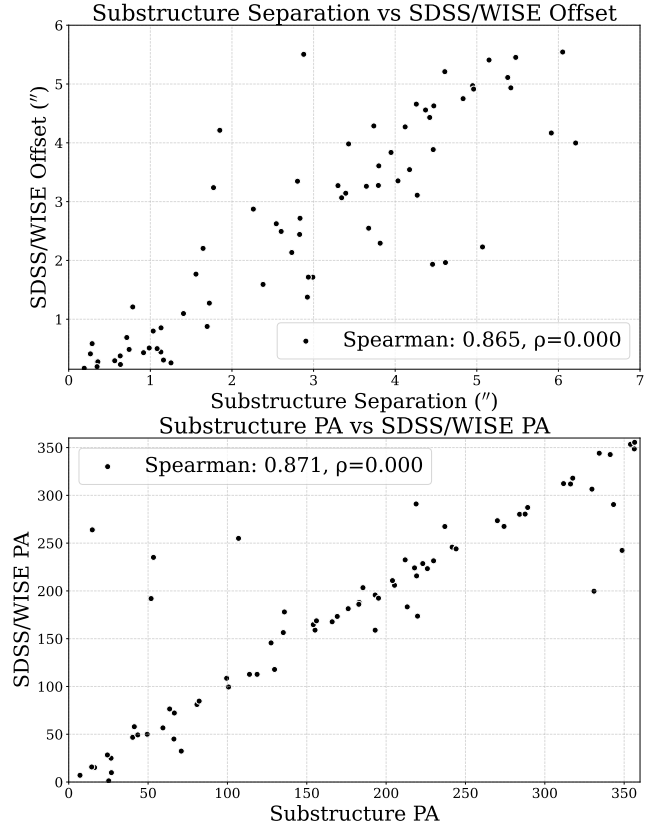


Figure 14. (Top) A comparison between the angular separations of the SDSS/WISE positional offset and substructure pair in each target with substructure. (Bottom) A comparison between the position angles of the SDSS/WISE positional offset and substructure pair in each target with substructure.

(offset $< 0.15''$; see Section 2.3). Only one target of the 11 contains substructure with a flux ratio of 0.185, which is consistent with the SDSS/WISE offset being necessary to enhance the detection of unresolved substructure. However, a larger sample is required to obtain a more robust test of the offset selection.

4.4. HST Observations

In the 48 target Keck merger sample (SDSS/WISE offset $< 1.5''$) there are 17 targets with publicly available HST optical images. We take advantage of the high resolution HST images to compare the optical and infrared morphologies of these targets. We find that the optical morphology of these targets is much more complex than what we see in the infrared imaging. The nuclear optical emission is often partially obscured and with clear signatures of dust lanes. Nuclear dust lanes are commonly seen in HST images of nearby AGNs (e.g. Malkan et al. 1998; Hunt & Malkan 2004). This partial obscuration appears to be the cause of SDSS/WISE offsets in many of the targets with no substructure, since the SDSS posi-

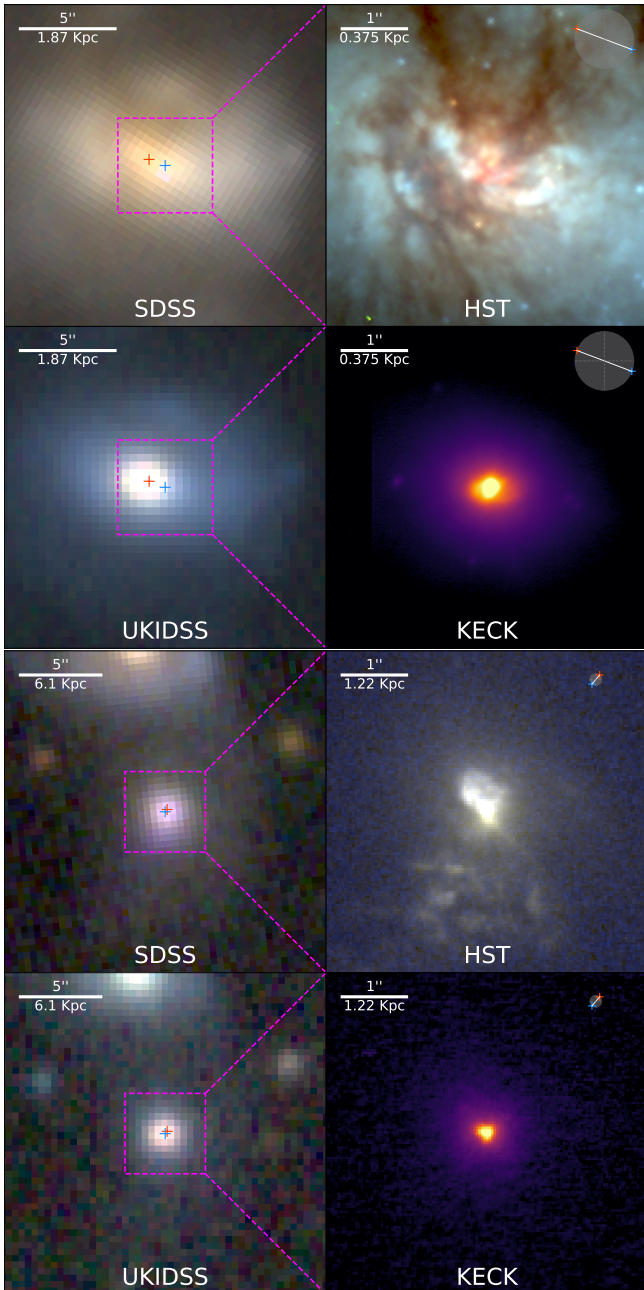


Figure 15. Examples of targets with no substructure whose SDSS/WISE offsets are likely caused by partial obscuration of their optical emission. For each target we include the corresponding SDSS, HST, Keck and when available UKIDSS images. In the top right of each HST or Keck image we include a representation of the SDSS/WISE offset which shows the orientation and length of the offset for that particular system, additionally we overlay the WISE (red) and SDSS (blue) coordinates onto the SDSS or UKIDSS images. The targets included, J083824 (Top) and J135429 (Bottom), are from the 48 target Keck merger sample.

tion will be biased towards unobscured nuclear emission and not necessarily the true location of the central nucleus. In Figures 15 and 16 we show examples of targets with no substructure detected in the Keck data, where the SDSS/WISE offsets are likely caused by partial obscuration. The SDSS/WISE offsets in these targets are oriented in the direction of the dust lanes and clouds present in the nuclear regions. Although this partial obscuration can lead to spurious SDSS/WISE offsets that do not correspond to genuine sources of emission in the Keck data, several of the targets with substructure also have HST imaging that shows partial obscuration of the nuclear region. In Figure 17 we show systems containing multiple near-infrared nuclei, where at least one nucleus is missing or obscured in the optical HST imaging. In these targets we also see that the SDSS/WISE offset is oriented such that the WISE coordinate likely corresponds to the obscured nucleus, suggesting that the offset is caused by this obscuration.

To further explore this relationship, we identify 18 targets from the expanded merger sample ($0.15'' < \text{SDSS/WISE offset} < 6''$) that have Keck and HST imaging data. In these targets we register the number of nuclear infrared and optical sources of emission and take the ratio of these quantities. In Figure 18 we show a histogram of these ratios split between mergers with nuclear separations below and above 3 kpc. We find that a higher fraction of early-stage mergers (i.e., those with nuclear separations > 3 kpc) exhibit ratios near unity, compared to late-stage mergers. This suggests that the nuclear regions of early-stage systems may be less obscured. However, the majority of targets in both early and late-stage mergers show flux ratios below one. This is likely due to dust lanes and clouds fragmenting the optical emission, creating the illusion of multiple sources. Crucially, these low ratios do not imply the presence of additional genuine nuclei in the optical images but rather reflect increased obscuration in the nuclear regions of merging galaxies that can mimic substructure. These findings demonstrate that high resolution optical surveys will incorrectly identify potential dual nuclei in late stage mergers. Indeed, sub-arcsecond offsets between UKIDSS and WISE, both of which are infrared surveys, are more likely to indicate a genuine dual nucleus as seen from Figure 19.

5. SUMMARY AND CONCLUSIONS

The goal of this work was to test a novel selection technique that leverages the astrometric precision of SDSS and WISE—two wide-field sky surveys—and to use positional offsets between these two surveys to identify unresolved substructure ($< 1.5''$) in late-stage, MIR color-selected mergers. These systems are promising candidates to host sub-kpc scale dual AGNs, a regime of parameter space that remains largely unexplored but is vital to our understanding of galaxy evolution, black hole growth, and the evolution of BSBHs and the detec-

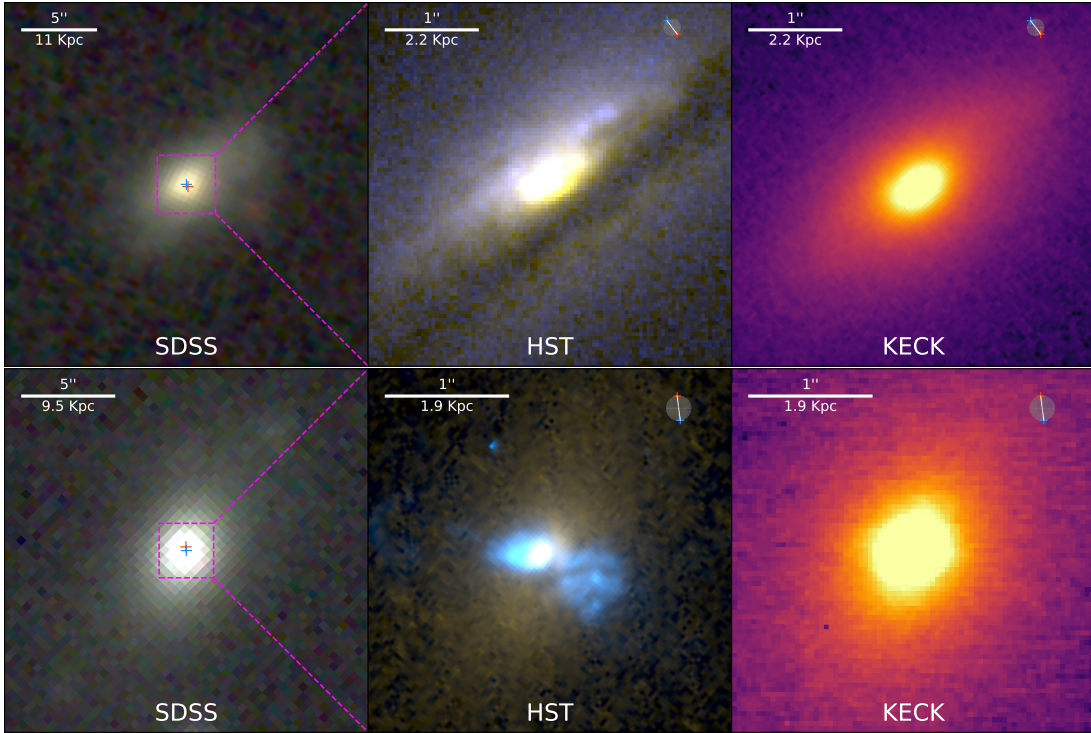


Figure 16. Same as Figure 15 except the targets included, J100654 (Top) and J165315 (Bottom), are from the Keck non-merger comparison sample.

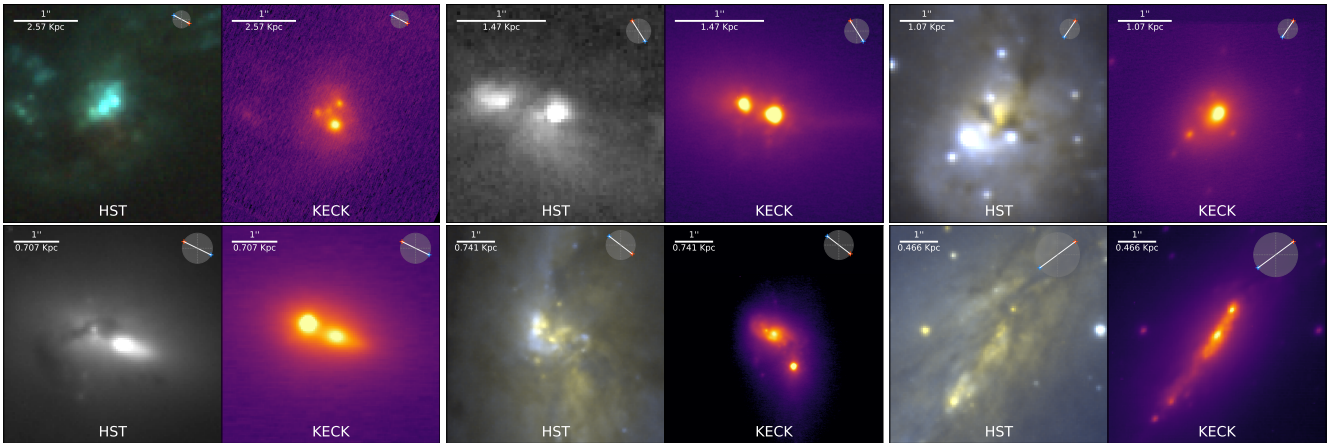


Figure 17. Example images of targets with substructure whose SDSS/WISE offsets are likely caused by partial obscuration of the substructure. For each target we include the corresponding HST and Keck images. In the top right of each image we include a representation of the SDSS/WISE offset which shows the orientation and length of the offset for that particular system. (Top Left) J015028, (Top Middle) J110213, (Top Right) J152659, (Bottom Left) J131517 (Bottom Middle) J134442, (Bottom Right) J132035.

tion rates of GWs by LISA. To evaluate the effectiveness of this method, we conducted a high-resolution adaptive optics study of 48 mergers exhibiting red WISE colors ($W_1 - W_2 > 0.5$; Blecha et al. 2018) and significant SDSS/WISE positional offsets ($0.15'' < \text{offset} < 1.5''$). These offsets suggest the presence of previously unresolved nuclear substructure and at least one actively accreting AGN. Our primary objective was to deter-

mine whether this offset-based selection technique reliably identifies mergers with compact, unresolved components, potentially indicative of sub-kpc dual AGNs and worthy of further spatially resolved follow-up. The results of our analysis are as follows:

1. Our results revealed that a significant fraction (20/48 or 42%) of the Keck merger sample (SDSS/WISE offset $< 1.5''$) showed substructure

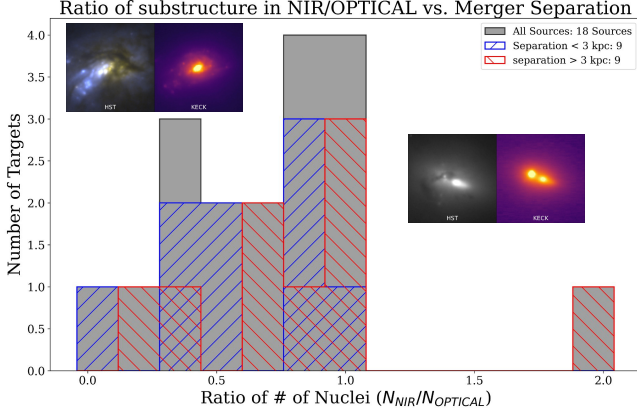


Figure 18. Histogram of the ratio of NIR/Optical sources as a function of merger nuclear separation for targets in our 48 target merger sample with NIRC2 and HST imaging. We include images of two targets included in this plot, J131534 and J131517, as an example of targets with a ratio above and below 1, respectively.

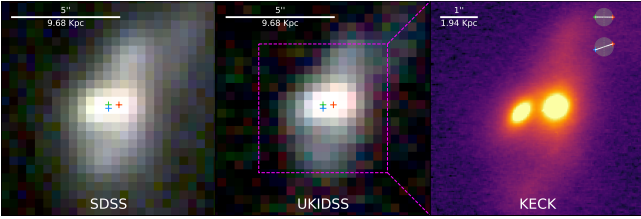


Figure 19. SDSS and NIRC2 image of J001707, a target from the Keck merger sample with a sub-arcsecond offset between its WISE and UKIDSS nuclear coordinates. Overlaid on the SDSS image is the WISE coordinate (red), SDSS coordinate (blue) and UKIDSS coordinate (green). In the top right of the NIRC2 image we include representations of the SDSS/WISE and UKIDSS/WISE offsets corresponding to their sizes and orientations. Similarly to the SDSS/WISE offset, the UKIDSS/WISE offset traces the dual nuclei revealed in the Keck image. The UKIDSS coordinate is not nearly as affected by obscuration as the SDSS coordinate, thus an offset between UKIDSS and WISE is more likely to reflect real substructure.

ture unresolved by SDSS, demonstrating that our methodology is a promising pathway to find dual AGN with follow-up spectroscopy.

2. Because the field of view of our NIRC2 images is too small to include nearby reference stars, we are unable to determine an accurate World Coordinate System (WCS) for the Keck data. This prevents a direct spatial mapping between detector pixels and sky coordinates, making it difficult to verify whether the SDSS/WISE offsets align precisely with the substructures revealed in the Keck adaptive optics (AO) images. Nevertheless, we

find a strong correlation between both the orientation and separation of the SDSS/WISE offsets and those of the substructure pairs identified in the Keck data, suggesting that the SDSS/WISE offsets are indeed tracing the unresolved sources of emission detected by Keck. Furthermore, we observe that the detection rate of unresolved substructure does not decline with decreasing offset size, indicating that non-detections are unlikely to result from limitations in the astrometric precision of SDSS or WISE.

3. For targets in our sample where no substructure is detected in the Keck AO data, we find that many of the observed SDSS/WISE positional offsets can be attributed to partial obscuration of the nuclear regions in these mergers. This obscuration affects the optical emission more strongly than the infrared, leading to mismatches between the SDSS (optical) and WISE (infrared) centroid positions, rather than indicating true substructure. This interpretation is supported by HST optical imaging of a subset of our sample, which reveals prominent dust lanes and clouds in many of these systems. Moreover, the alignment between the SDSS/WISE offset direction and the orientation of the dust distribution further suggests that patchy obscuration in the nuclear regions is responsible for the astrometric offsets in the targets in which no substructure is detected in the infrared. We also note that optical HST imaging reveals clumps of emission that are absent in the infrared AO observations indicating that high resolution optical surveys will incorrectly identify potential dual nuclei in late stage mergers in which only one nuclei is present.
4. Targets in which substructure is identified in the infrared tend to exhibit higher extinction, as indicated by elevated $E(B-V)$ values, compared to those without detected substructure. This suggests that late-stage mergers with nuclear pair separations < 1 kpc are often heavily obscured. HST imaging of several targets with infrared substructure reveal that some of the sources of emission seen in the infrared data is absent in the optical, further supporting a scenario in which the nuclear regions of late stage mergers are heavily obscured.
5. We constructed a comparison sample of NIRC2 imaged galaxies that are not identified as mergers by Galaxy Zoo and show no visual signs of interaction in their SDSS images. This sample was selected to match our merger sample using the same WISE color, magnitude, and SDSS/WISE offset criteria, allowing us to test whether the substructure detected in our Keck AO data is truly associated with SDSS/WISE offsets rather than a random outcome of selecting red MIR color se-

lected mergers. We find that 23% of the non-merging galaxy sample also exhibit substructure in the Keck AO data, indicating that SDSS/WISE positional offsets can reveal unresolved components even in systems not classified as mergers by Galaxy Zoo. This may indicate that the morphological indicators of the merger may not be apparent in SDSS for systems with dual AGNs at sub-kpc pair separations. Indeed, SMBH binary merger timescales are highly uncertain, with some simulations predicting that the SMBHs merge long after the host galaxies have coalesced at a stage when the morphological signs of the galaxy merger may have faded, but the black holes remain dynamically distinct (e.g. [Volonteri et al. 2020](#)). The offset technique we employ may therefore be a way to select larger samples of late-stage mergers in which the merger signatures are no longer apparent in their SDSS images.

6. Interestingly, we find that in the 48 target Keck merger sample the majority of targets with substructure are classified as AGNs or composites based on their SDSS spectra, and have the reddest $W_2 - W_3$ colors indicating substantial obscured star formation activity. Of the targets with $W_2 - W_3$ colors > 4.2 , 73% contain substructure.

Further spectroscopic analysis of the targets containing substructure is needed to confirm the presence of dual AGN in this sample. Follow-up OH-Suppressing Infrared Imaging Spectrograph (OSIRIS) K-band Integral Field Spectroscopy (IFS) observations of a subset of the sample will be presented by McDonald et al. (in preparation).

The combined optical and infrared observations presented in this work demonstrate that large-scale optical surveys are not effective for identifying closely separated nuclei in late-stage mergers. Due to significant dust obscuration at these advanced merger stages, studies targeting sub-kpc pair separations must be conducted in the infrared. Future wide-field infrared missions, such as the Nancy Grace Roman Space Telescope, have the potential to advance this field by probing even smaller nuclear separations. Additionally, the varstrometry technique—originally developed using Gaia data—may be adapted for use in the infrared, where the effects of dust are substantially reduced.

We emphasize that identifying closely separated nuclei in late-stage mergers is important regardless of whether they host dual AGNs. These systems represent a critical phase in the merger process, marked by intense star formation, significant morphological transformation, and potentially powerful feedback. Follow-up observations to investigate the nature of nuclear star clusters, molecular gas content, and outflows are essential for advancing our understanding of this key stage in galaxy evolution.

6. ACKNOWLEDGEMENTS

Camilo Vazquez acknowledges support from the Presidential Scholarship from George Mason University. R. W. P. gratefully acknowledges support through an appointment to the NASA Postdoctoral Program at Goddard Space Flight Center, administered by ORAU through a contract with NASA. Basic research in radio astronomy at the U.S. Naval Research Laboratory is supported by 6.1 Base Funding. F.M-S. acknowledges support from NASA through award 80NSSC23K1529. J.D.M’s research was supported by an appointment to the NASA Postdoctoral Program at the NASA Goddard Space Flight Center, administered by Oak Ridge Associated Universities under contract with NASA.

This research made use of Astropy,² a community-developed core Python package for Astronomy ([Astropy Collaboration et al. 2013](#)), as well as TOPCAT ([Taylor 2005](#)). The geometrical distortion correction code was run on ARGO and HOPPER, research computing clusters provided by the Office of Research Computing at George Mason University, VA. (<http://orc.gmu.edu>).

Some of the data presented herein were obtained at Keck Observatory, which is a private 501(c)3 non-profit organization operated as a scientific partnership among the California Institute of Technology, the University of California, and the National Aeronautics and Space Administration. The Observatory was made possible by the generous financial support of the W. M. Keck Foundation. The authors wish to recognize and acknowledge the very significant cultural role and reverence that the summit of Maunakea has always had within the Native Hawaiian community. We are most fortunate to have the opportunity to conduct observations from this mountain. This research has made use of the Keck Observatory Archive (KOA), which is operated by the W. M. Keck Observatory and the NASA Exoplanet Science Institute (NExSci), under contract with the National Aeronautics and Space Administration.

Funding for the Sloan Digital Sky Survey (SDSS) and SDSS-II has been provided by the Alfred P. Sloan Foundation, the Participating Institutions, the National Science Foundation, the U.S. Department of Energy, the National Aeronautics and Space Administration, the Japanese Monbukagakusho, and the Max Planck Society, and the Higher Education Funding Council for England. The SDSS Web site is <http://www.sdss.org/>. The SDSS is managed by the Astrophysical Research Consortium (ARC) for the Participating Institutions. The Participating Institutions are the American Museum of Natural History, Astrophysical Institute Potsdam, University of Basel, University of Cambridge, Case Western Reserve University, The University of Chicago, Drexel University, Fermilab, the Institute for Advanced Study,

² <http://www.astropy.org>

the Japan Participation Group, The Johns Hopkins University, the Joint Institute for Nuclear Astrophysics, the Kavli Institute for Particle Astrophysics and Cosmology, the Korean Scientist Group, the Chinese Academy of Sciences (LAMOST), Los Alamos National Laboratory, the Max-Planck-Institute for Astronomy (MPIA), the Max-Planck-Institute for Astrophysics (MPA), New Mexico State University, Ohio State University, University of Pittsburgh, University of Portsmouth, Princeton University, the United States Naval Observatory, and the University of Washington. The HST data were obtained from the Mikulski Archive for Space Telescopes at the Space Telescope Science Institute, which is operated by the Association of Universities for Research in Astronomy, Inc.

This publication makes use of data products from the Wide-field Infrared Survey Explorer, which is a joint project of the University of California, Los Angeles, and the Jet Propulsion Laboratory/California Institute of Technology, funded by the National Aeronautics and Space Administration.

The UKIDSS project is defined in [Lawrence et al. \(2007\)](#). UKIDSS uses the UKIRT Wide Field Camera (WFCAM; [Casali et al. 2007](#)) and a photometric system described in [Hewett et al. \(2006\)](#). The pipeline processing and science archive are described in [Irwin \(2008\)](#) and [Hambly et al. \(2008\)](#). We have used data from the 9th data release, which is described in detail in [Lawrence et al. \(2007\)](#).

Software: Astropy ([Astropy Collaboration et al. 2013](#)), NumPy, ([Harris et al. 2020](#)) SciPy, ([Virtanen et al. 2020](#)) TOPCAT ([Taylor 2005](#)),

APPENDIX

A. SUBSTRUCTURE TARGETS

In the following section, we present the results and analysis for all 20 targets with substructure detected with NIRC2 imaging. For each target, we show its SDSS *irg* image, NIRC2 image, and when available, its UKIDSS *KHY* image and/or HST image; for targets with HST observations in multiple filters we show a three color image. Each image is aligned with North pointing up and East to the left. For each SDSS and UKIDSS image we include a white scale bar – corresponding to $5''$ – in the top left and overlay the system’s SDSS coordinate in blue and WISE coordinate in red. We also include a magenta square in either/both the SDSS and UKIDSS images that corresponds to the size and location of the Keck image and HST image when available. In each NIRC2 and HST image we include a white scale bar – corresponding to $1''$ – in the top left and a visual representation of the SDSS/WISE offset in the top right, corresponding to the distance between the SDSS (blue) and WISE (red) coordinates and their orientation relative to each other. We do not present the location of the SDSS and WISE coordinates in these images because there are no stars within the FOV of the images and thus we are unable spatially map between detector pixels and sky coordinates.

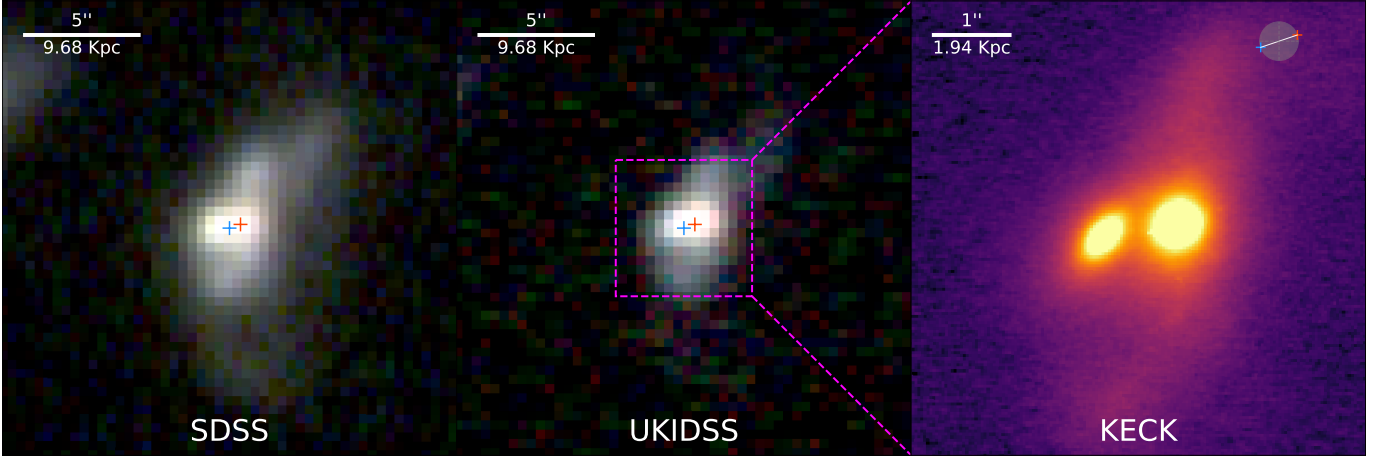
A.1. *J001707+011506*

Figure 20. Images provided above are described at the beginning of Appendix A.

NIRC2 imaging of J001707 reveals that it contains clear dual nuclei separated by $0.986''$ or 1.910 kpc with a PA of 99.51° . In both SDSS and UKIDSS these nuclei are blended into a single apparent nucleus elongated along the direction of the two nuclei. The host galaxy exhibits bipolar tidal tails extending out to ~ 12.4 kpc in the North and ~ 5.6 kpc in the South. The SDSS/WISE offset detected in this target has a separation of $0.511''$ and PA of 108.6° . The SDSS/WISE offset detected in this merger system clearly corresponds to the dual nuclei as the PAs of the SDSS/WISE offset and nuclear pair are very similar, although the separation of the nuclei is underpredicted by the SDSS/WISE offset (see Section 4.2)(i.e. $\Delta Sep. = 0.475''$ and $\Delta PA = 9.09^\circ$). The host galaxy of this object is optically classified as a K_{01} type AGN in the MPA-JHU catalog. Additionally, it lies within the AGN classification of our BPT diagram and within the Jarrett AGN region of our WISE color-color diagram suggesting it is a candidate dual AGN.

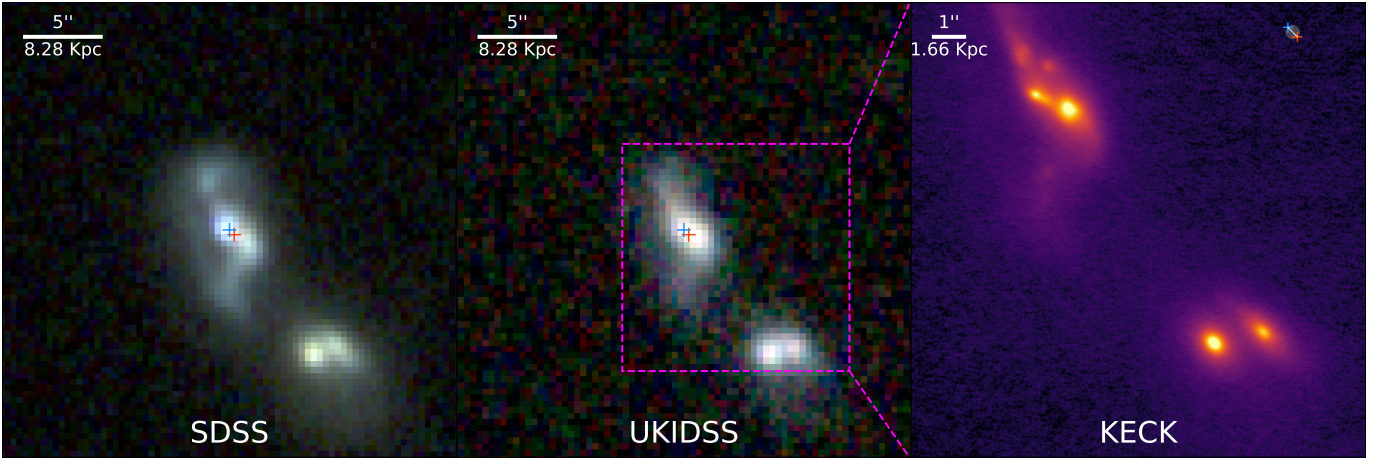
A.2. *J010942-004417*

Figure 21. Images provided above are described at the beginning of Appendix A.

J010942 appears to be a highly disturbed galaxy undergoing a merger with a companion $10''$ or 16.57 kpc to the Southwest. J010942 appears to contain a single elongated nucleus in both SDSS and UKIDSS whereas the companion contains two semi-resolved nuclei. High-resolution NIRC2 imaging of this target reveals two nuclei and confirms the presence of two nuclei in the companion. Inspection of SDSS DR16 spectra of J010942 and its companion reveals a velocity difference of ~ 70 km/s suggesting that they are associated with each other, although higher resolution spectroscopic follow-up is required for confirmation (McDonald et al. in prep.). The two nuclei in J010942 are separated by $1.129''$ or 1.871 kpc with a PA of 246.3° . The SDSS/WISE offset detected in the target has a separation

of $0.443''$ and PA of 225° which underpredicts the separation of the dual nuclei (see Section 4.2) but more closely follows the orientation of the nuclei (i.e. $\Delta Sep. = 0.686''$ and $\Delta PA = 21.30^\circ$). Comparison between the SDSS and UKIDSS cutout images of this target shows that the apparent nucleus of the optical and near-infrared emission of this target are clearly offset from each other and thus driving the SDSS/WISE offset. However, high resolution optical imaging is required to determine whether this discrepancy is caused by partial obscuration or an inherent difference in the emission properties of the two nuclei. The host galaxy of J010942 is optically classified as a K_{03} type AGN in the MPA-JHU catalog. Additionally, it lies within the composite classification of our BPT diagram and outside of the Jarrett AGN region of our WISE color-color diagram which may suggest that these two nuclei are not dual AGN but rather a single AGN and a non-AGN (i.e. inactive-SMBH or star forming region).

A.3. J015028+130858

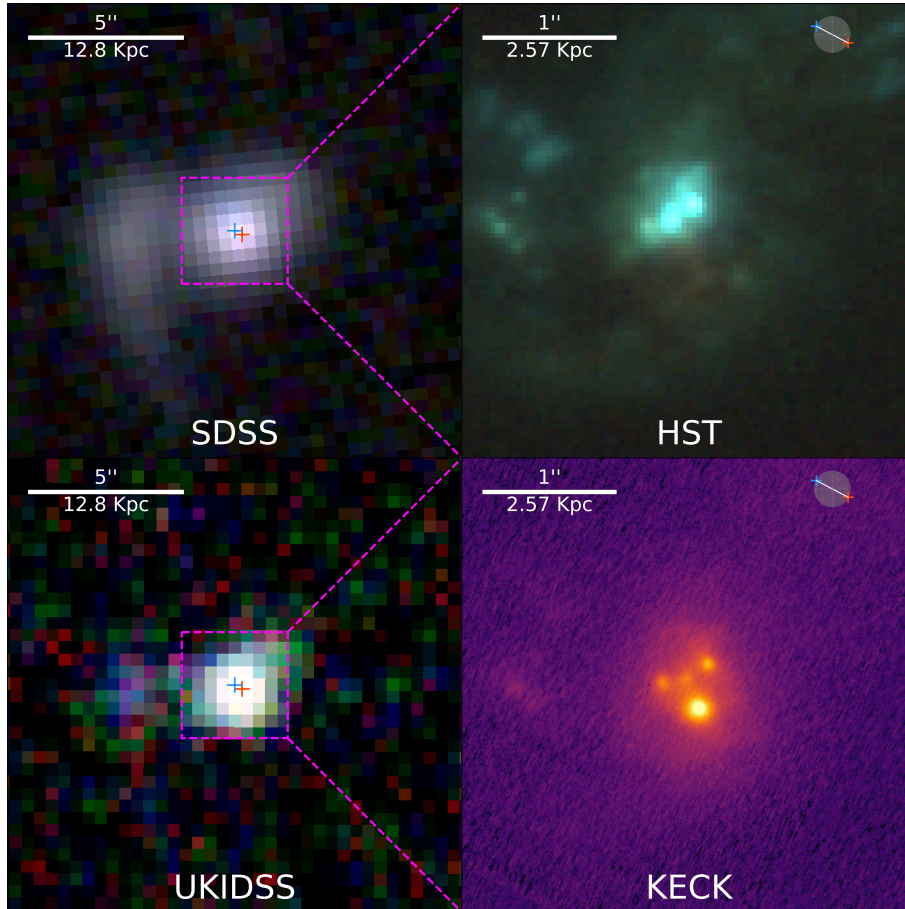


Figure 22. Images provided above are described at the beginning of Appendix A.

J015028 is a merger system with a galaxy pair in the East and West of the SDSS cutout image, only the Western galaxy is visible in UKIDSS, separated by $3.742''$ or 9.60 kpc. We detect an SDSS/WISE offset in this Western galaxy with a separation of $0.275''$ and PA of 62.35° and thus consider it to be the target galaxy for this analysis. High resolution NIRC2 imaging of the target reveals three sources of significant near-infrared emission in the central nuclear region forming a triangle with a bright southern source and two dimmer sources to the Northeast and Northwest. Inspection of the archival HST WFC3 imaging of this target (Program No. 12310; F390W, F475W and F850LP) reveals that the brightest source in the near-infrared is not visible at optical wavelengths, most likely due to obscuration from dust. Based on the orientation of the substructure in the near-infrared and optical it can also be seen that there is a fourth source of emission seen in the HST image which corresponds to the region between the two Northern sources in the NIRC2 image. The orientation of the SDSS/WISE offset visually suggests that the WISE coordinate is tracing the position of the bright Southern source of near-infrared emission and the SDSS coordinate is tracing the unobscured optical emission in the North, creating the SDSS/WISE offset we detect. Our comparison of the separation

and PA of the SDSS/WISE offset with the substructure in this target yielded very similar separations but a significant difference in PA (i.e. $\Delta Sep. = 0.072''$ and $\Delta PA = 106.299^\circ$). This is due to the fact that the substructure pair is defined based on the brightest secondary source of near-infrared emission, which in this case is not necessarily the brightest secondary source of optical emission. The host galaxy of J015028 is optically classified as a S_{06} type AGN in the MPA-JHU catalog. Additionally, it lies within the star-forming classification of our BPT diagram and outside of the Jarrett AGN region of our WISE color-color diagram which may suggest that the compact sources of emission in this target are star forming regions rather than galaxy nuclei or AGN.

A.4. J082312+275140

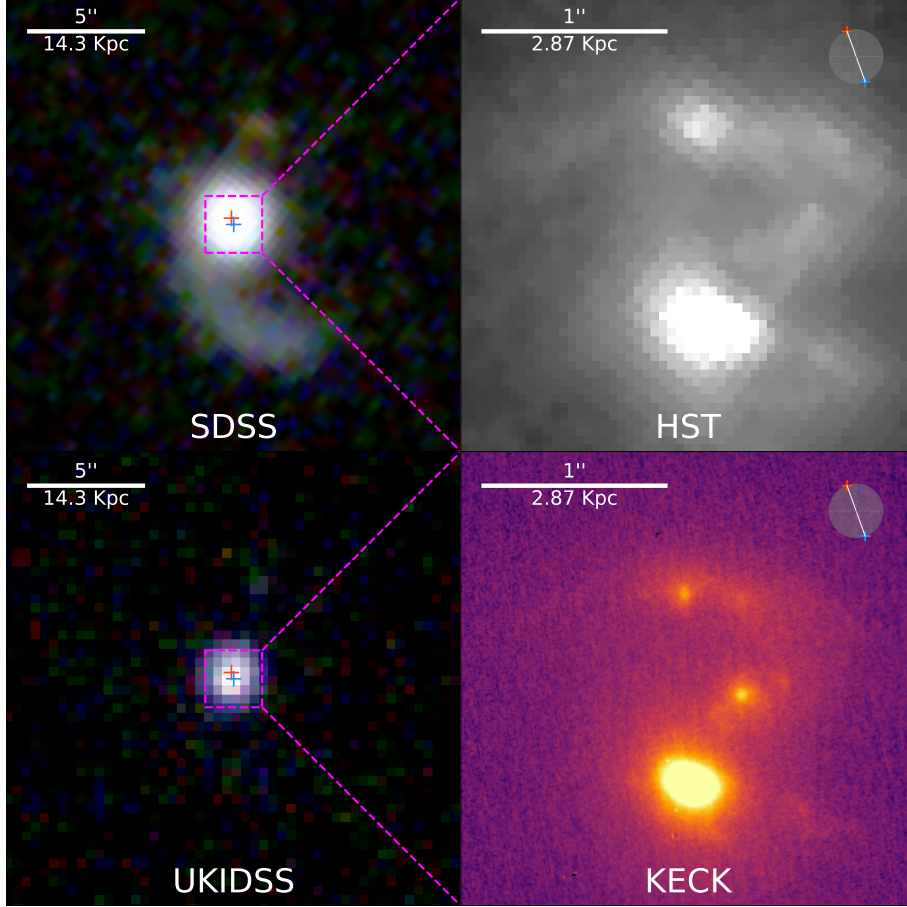


Figure 23. Images provided above are described at the beginning of Appendix A.

NIRC2 imaging of J082312 reveals three potential nuclei connected by an arc of emission. There is a clear primary nucleus and two secondary nuclei, northwest from the primary at a distance of $0.56''$ and north from the primary at a distance of $1.06''$ with PA's of 331.030° and 2.440° respectively. The host galaxy, as seen in SDSS, exhibits a tidal tail that extends out to ~ 25 kpc and curves towards the West, however in UKIDSS it is a point source. The HST WFPC2 imaging survey conducted by [Borne et al. \(1999\)](#) included F814w observations of J082312. The same arc of emission and broad tidal tail can be seen in the HST image, however only two of the three nuclei are visible with a pair separation of $\sim 1''$, indicating that the Northwestern nucleus is obscured. The Northwestern nucleus is the brightest of the secondary nuclei, thus we identify the primary and this secondary nucleus as the substructure pair in this target. The SDSS/WISE coordinate offset has a separation of $0.294''$ and PA of 199.741° . Although the orientation of the SDSS/WISE offset does not seem to trace that of the substructure pair, it appears to have a similar orientation to that of the more separated secondary. The host galaxy of this object is optically classified as a K_{03} type AGN in the MPA-JHU catalog. Additionally, it lies within the composite classification of our BPT diagram and outside of the Jarrett AGN region of our WISE color-color diagram.

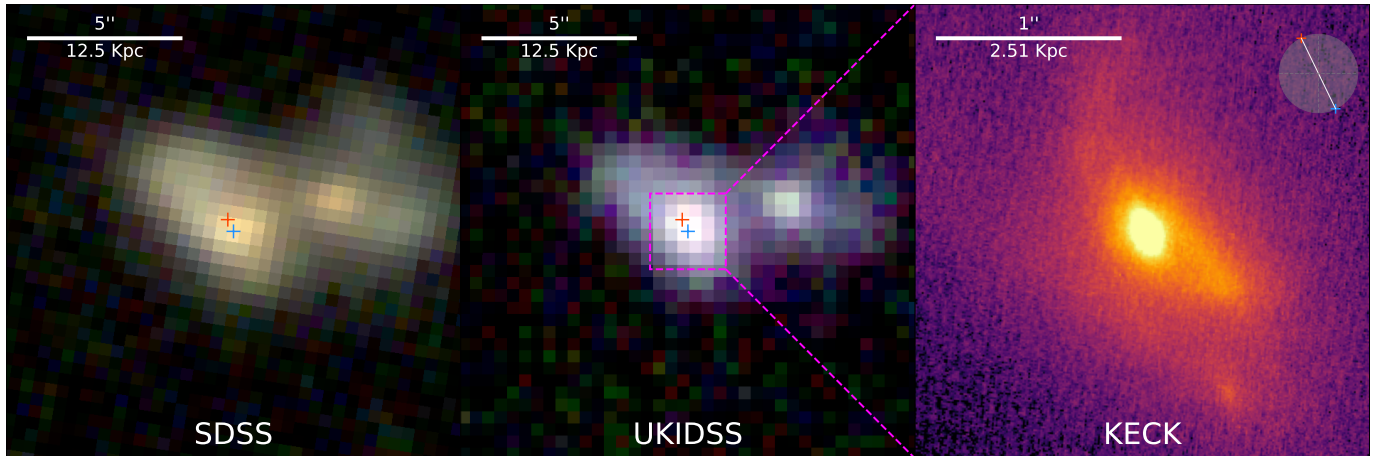
A.5. *J091529+090601*

Figure 24. Images provided above are described at the beginning of Appendix A.

J091529 is a close galaxy pair separated by $3.344''$ and 8.392 kpc; the nuclei of both galaxies are resolved in the SDSS, UKIDSS and NIRC2 images. The high resolution NIRC2 imaging of this target reveals previously unresolved substructure near the primary central nucleus of the Eastern galaxy. Surrounding this nucleus we can see faint emission consistent with bipolar tidal tails curving into the North and Southwest, most likely generated by the ongoing galaxy merger. There is one faint secondary source of emission within a $1.5''$ radius of the primary central nucleus of the Eastern galaxy. This substructure lies at a distance of $0.917''$ or 2.300 kpc Southwest from the primary with a PA of 205.302° . Although this substructure does not appear to be a secondary nucleus it does seem to trace the SDSS/WISE offset. The SDSS/WISE offset underpredicts the separation of the substructure as expected (see Section 4.2) with a separation of $0.431''$ but the PA of 205.880° is very similar to that of the substructure pair. We note that there is another SDSS/WISE offset detected in this merger system with a separation of $3.066''$ between the SDSS coordinate of the Eastern galaxy and the WISE coordinate which coincides with the position of the Western galaxy. Since this offset is resolvable by SDSS and UKIDSS and corresponds to a secondary galaxy resolvable by SDSS, we do not consider it a detection of substructure in the target galaxy. The host galaxy of this object is optically classified as a K_{01} type AGN in the MPA-JHU catalog. Additionally, it lies within the AGN classification of our BPT diagram and within the Jarrett AGN region of our WISE color-color diagram.

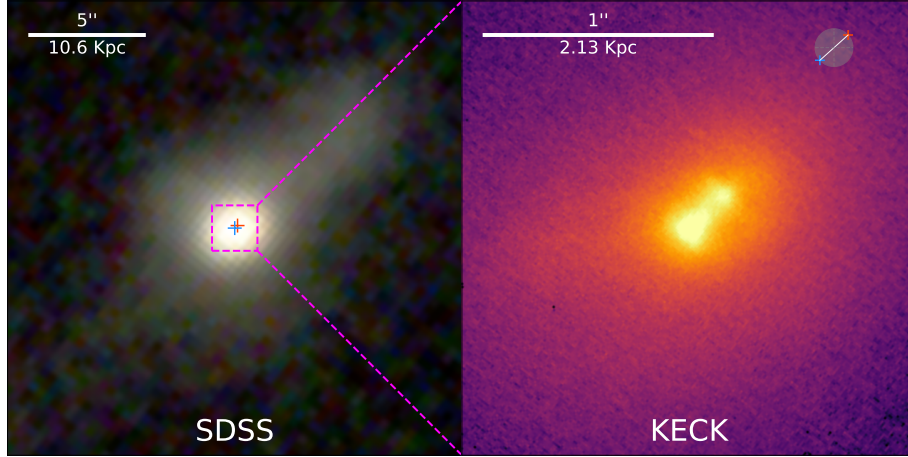
A.6. *J093314+630945*

Figure 25. Images provided above are described at the beginning of Appendix A.

J093314 is an advanced merger system which appears to contain a single nucleus with multiple tidal tails in its SDSS image. The tidal tails extend in opposite directions without much curvature out to distances of ~ 30 kpc and ~ 15 kpc. The NIRC2 imaging reveals two apparent nuclei at a separation of $0.190''$ or 0.405 kpc with a PA of 316.231° . The separation and PA of the SDSS/WISE offset detected in this target are $0.167''$ and 311.876° . It is clear that our offset selection detected unresolved dual nuclei in this system but is also closely traced by the actual separation and PA between these nuclei (i.e. $\Delta Sep. = 0.023''$ and $\Delta PA = 4.355^\circ$). The host galaxy of this object is optically classified as a K_{01} type AGN in the MPA-JHU catalog. Additionally, it lies within the AGN classification of our BPT diagram and within the Jarrett AGN region of our WISE color-color diagram, suggesting this may be a candidate dual AGN system.

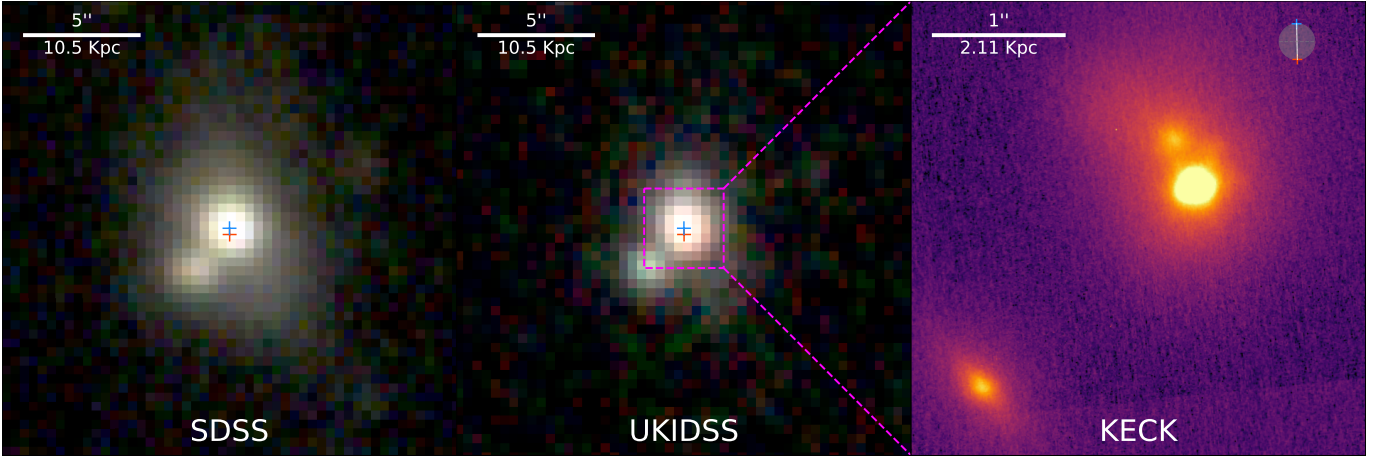
A.7. *J101653+002856*

Figure 26. Images provided above are described at the beginning of Appendix A.

J101653 is a close galaxy pair separated by $2.26''$ or 4.76 kpc, with the nuclei of both galaxies resolved in SDSS and UKIDSS. This target has been previously identified as an elliptical galaxy within a disturbed pre-coalescence system (Pierce et al. 2023). The detected SDSS/WISE offset is in the Northwestern galaxy of this pair. The NIRC2 imaging of the Northwestern galaxy reveals a third source of emission very close to its primary central nucleus. The separation between this close pair is $0.350''$ or 0.737 kpc with a PA of 25.195° . The separation and PA of the SDSS/WISE offset are $0.275''$ and 1.251° . The size and PA of the SDSS/WISE offset is similar to that of the substructure pair although with less accuracy than other targets in this sample. Additionally, we note that based on the orientation of the offset

it appears that the WISE coordinate corresponds to the primary central nucleus and the SDSS coordinate corresponds to the secondary nucleus. This may suggest that the primary nucleus is obscured, however higher resolution optical imaging is required to confirm this. The host galaxy of this object is optically classified as a K_{01} type AGN in the MPA-JHU catalog. Additionally, it lies within the AGN classification of our BPT diagram and within the Jarrett AGN region of our WISE color-color diagram.

A.8. $J110213+645925$

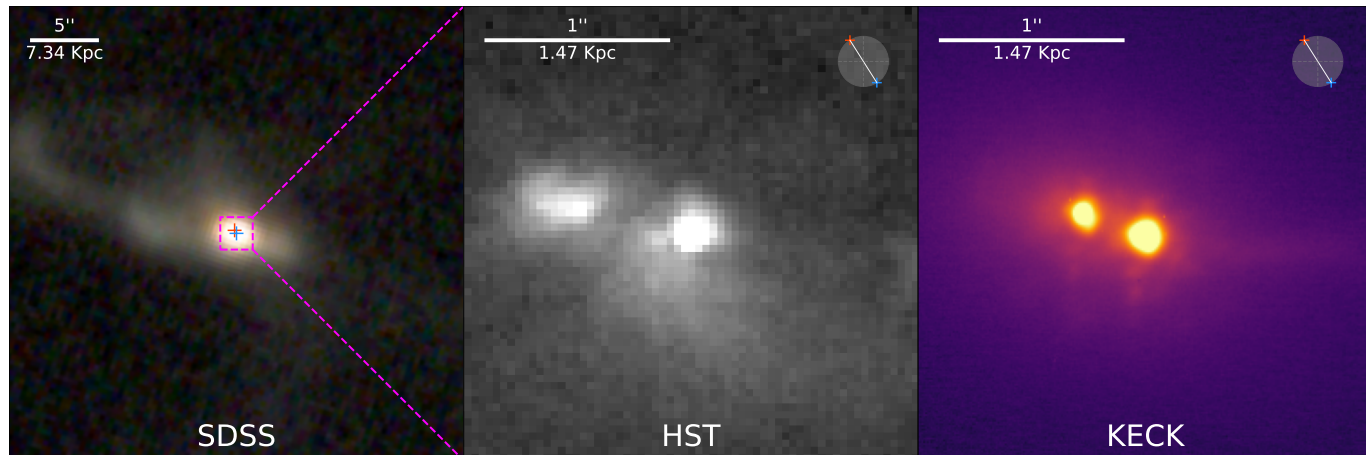


Figure 27. Images provided above are described at the beginning of Appendix A.

$J110213$ is a candidate dual AGN system containing clear sub-kpc dual nuclei with a separation of $0.357''$ or 0.524 kpc and PA of 70.923° . This is a late-stage merging system with one apparent nucleus detected in SDSS. One prominent tidal tail extends $17.5''$ out to the East and curves towards the North and back into the center of the galaxy forming a closed loop. [Zhao et al. \(2019\)](#) imaged this target with the Hubble Space Telescope WFC3 camera (F105W and F438W), classifying it as a type 2 quasar within a merging system. Upon inspection of the HST images, two nuclei are visible with an apparent dust lane between them. However, these nuclei have much more irregular shapes than what is seen in our Keck image and the separation of the apparent nuclei in the optical F438W image is $\sim 0.67''$. It is possible that the dust lane is partially obscuring one of the nuclei in the optical image causing this discrepancy. If we assume the Western nucleus is the same source in both the NIRC2 and HST image then the location of the Eastern nucleus (in the NIRC2 image) coincides with the dust lane. Furthermore, we note that based on the orientation of the SDSS/WISE offset the WISE coordinate coincides with the obscured Eastern nucleus and the Galaxy Zoo position coincides with the Western nucleus. An obscuration of the Eastern nucleus would best account for the orientation and positioning of the offset since the Eastern nucleus would only be detected in WISE. Additionally, the separation and PA of the SDSS/WISE offset in $J110213$ is $0.276''$ and 32.363° which is similar the separation and PA of the dual nuclei. The host galaxy of this object is optically classified as a K_{01} type AGN in the MPA-JHU catalog. Additionally, it lies within the AGN classification of our BPT diagram and within the Jarrett AGN region of our WISE color-color diagram making this a strong candidate dual AGN system.

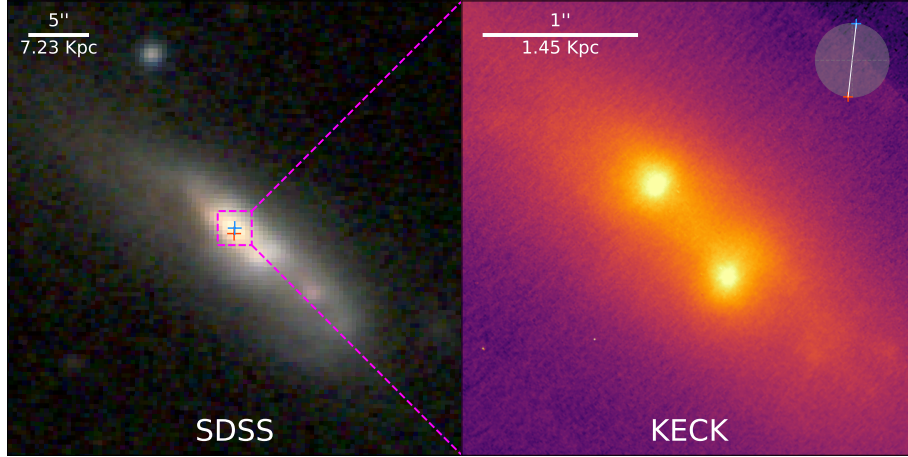
A.9. *J120408+132116*

Figure 28. Images provided above are described at the beginning of Appendix A.

J120408 is a candidate dual AGN system containing two clear nuclei at a separation of $0.740''$ or 1.070 kpc and PA of 219.846° . SDSS imaging of this target shows an elongated galaxy with one apparent optical nucleus and a highly extended ($> 10''$) tidal tail extending to the Northeast. The SDSS/WISE offset for this target has a separation of $0.486''$ and PA of 173.630° . This does not trace the observed properties of the dual nuclei well, but nonetheless was able to detect them within an apparent single nuclei system. The host galaxy of this object is optically classified as a K_{01} type AGN in the MPA-JHU catalog. Additionally, it lies within the AGN classification of our BPT diagram and outside of the Jarrett AGN region of our WISE color-color diagram.

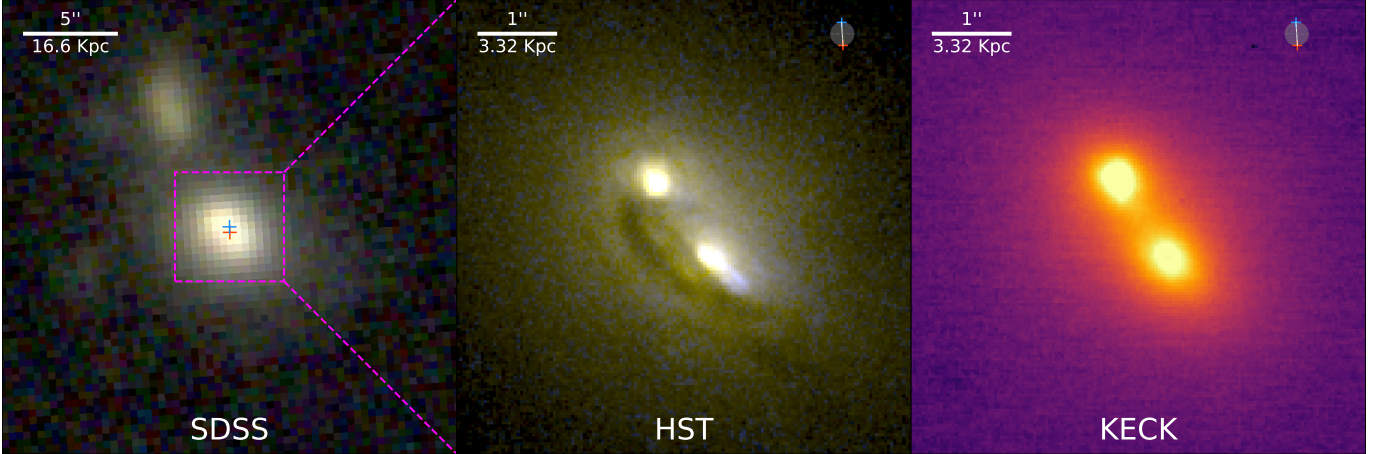
A.10. *J123915+531414*

Figure 29. Images provided above are described at the beginning of Appendix A.

J123915 is one of the targets in the 48 target Keck merger sample which has publicly available NIRC2 imaging available in the Keck archive (see Section 2.1). Fu et al. (2011a) conducted Keck LGSAO observations of this target with the NIRC2 Wide-Field Camera (FOV: $40'' \times 40''$, pixel scale: $0.039686'' \text{pixel}^{-1}$) in the K_p filter as part of an observing program searching for kpc-scale dual AGNs in double-peaked [OIII] AGNs. Additionally, this target was included in HST F438W and F814W observations of AGN with double-peaked narrow emission lines presented in Comerford et al. (2015), where they identify J123915 as a candidate dual AGN. The SDSS imaging of this target shows a galaxy with an unresolved and elongated bright central nucleus with a nearby galaxy in the Northeast likely to be unassociated ($\Delta v \sim 14800$ km/s). In both the NIRC2 and HST imaging we see clear dual nuclei at a separation of $1.161''$ or 3.855 kpc and PA of 213.349° , as measured in the NIRC2 image. In the HST image there is a clear

dust lane appearing to encircle and partially obscuring the Southwestern nucleus. The SDSS/WISE offset detected in this system has a separation of $0.306''$ and PA of 183.300° , poorly tracing the orientation and separation of the two nuclei (i.e. $\Delta Sep. = 0.855''$ and $\Delta PA = 30.049^\circ$). The SDSS/WISE offset may be tracing the obscuring dust lane with the SDSS coordinate coinciding with the region between the two nuclei but above the obscuring dust and the WISE coordinate coinciding with the region between the two nuclei being obscured by the dust lane. Interestingly, Comerford et al. (2015) show that the double-peaked emission lines seen in J123915 correspond to two [OIII] $\lambda 5007$ emission components separated by $0.39''$, which is similar to the separation of the SDSS/WISE offset we detect. The host galaxy of this object is optically classified as a K_{01} type AGN in the MPA-JHU catalog. Additionally, it lies within the AGN classification of our BPT diagram and outside of the Jarrett AGN region of our WISE color-color diagram.

A.11. *J124117+273251*

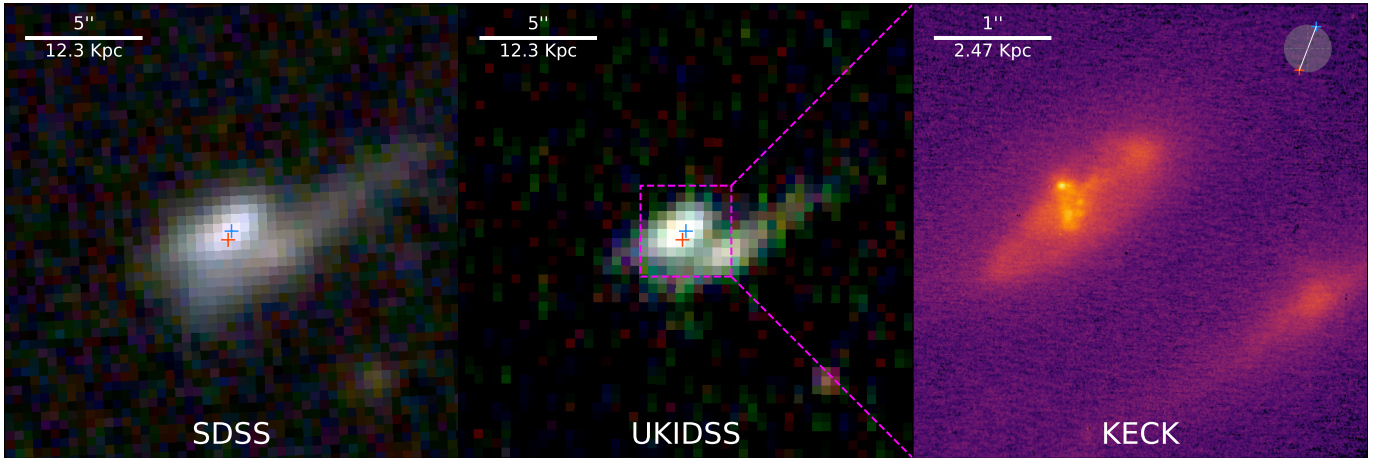


Figure 30. Images provided above are described at the beginning of Appendix A.

J124117 is the Northeastern galaxy in a close galaxy pair separated by $2.44''$ or 6 kpc, in which we detect a coordinate offset. Both galaxies are visible in the NIRC2 imaging, with the galaxy of interest (Northeast) containing a complex nuclear region with multiple compact sources of emission within the central arcsecond of the galaxy. The galaxy pair can be seen in SDSS and UKIDSS but the substructure in J124117 is unresolved in both surveys. The resolved substructure does not appear to be clear nuclei such as those in J110213 or J120408, the emission seems more consistent with extended nuclear emission that is partially obscured by a dust-lane. Although this target does not contain clear dual nuclei it does contain sub-arcsecond structure that seems to be traced by the offset measurement. The SDSS/WISE offset detected in this system has a separation of $0.411''$ and have a PA of 158.881° . Within the nuclear region of the primary galaxy we see two prominent “blobs” forming a substructure pair with a separation of $0.266''$ or 0.655 kpc and PA of 193.076° . The orientation of the SDSS/WISE offset does not appear to trace that of the candidate pair very well but it may be that the SDSS coordinate is biased towards the more extended emission in the galaxy (in the Northwest) and the WISE coordinate is more accurately detecting the bright nuclear emission in the South. The host galaxy of this object is optically classified as a K_{03} type AGN in the MPA-JHU catalog. Additionally, it lies within the composite classification of our BPT diagram and outside of the Jarrett AGN region of our WISE color-color diagram.

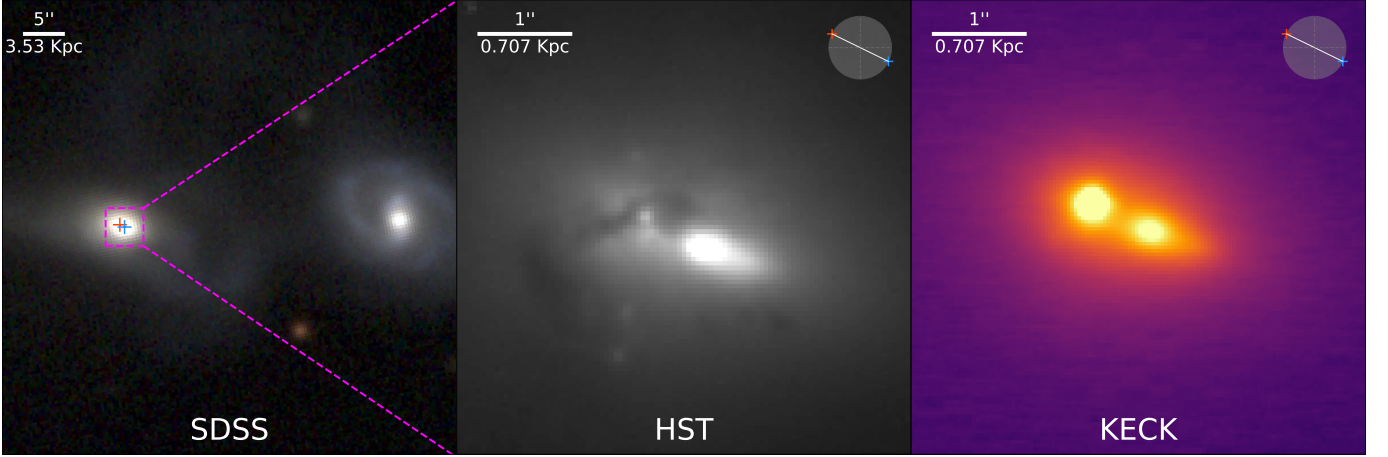
A.12. *J131517+442425*

Figure 31. Images provided above are described at the beginning of Appendix A.

J131517 is one of the targets in the 48 target Keck merger sample which has publicly available NIRC2 imaging in the Keck archive (see Section 2.1). Keck LGSAO observations of this target were conducted with the NIRC2 Wide-Field Camera (FOV: $40'' \times 40''$, pixel scale: $0.039686''\text{pixel}^{-1}$) in the K_p filter as part of Keck observing program Y076 in 2022. Additionally, this target was included in HST F814W observations of Swift-BAT AGN presented in Kim et al. (2021). In the SDSS cutout image we see that this target is part of an early stage merger system at a separation of $36.438''$ or 25.744 kpc, with the Eastern galaxy being the galaxy in which we detect an SDSS/WISE offset. The high resolution NIRC2 imaging reveals clear dual nuclei separated by $0.711''$ or 0.503 kpc and PA of 244.142° . The SDSS/WISE offset, with a separation of $0.689''$ and PA of 243.980° , very closely traces the orientation of the nuclear pair (i.e. $\Delta Sep. = 0.022''$ and $\Delta PA = 0.162^\circ$). Inspection of the HST F814W image of J131517 reveals that the Eastern nucleus of this pair is almost entirely obscured by a dust lane, which appears to be causing the significant offset between the WISE and SDSS nuclear coordinates. Furthermore, the orientation of the SDSS/WISE offset suggests that the WISE coordinate coincides with the optically obscured Eastern nucleus and the SDSS coordinate coincides with the unobscured Western nucleus. The host galaxy of this object is optically classified as a K_{03} type AGN in the MPA-JHU catalog. Additionally, it lies within the composite classification of our BPT diagram and within the Jarrett AGN region of our WISE color-color diagram.

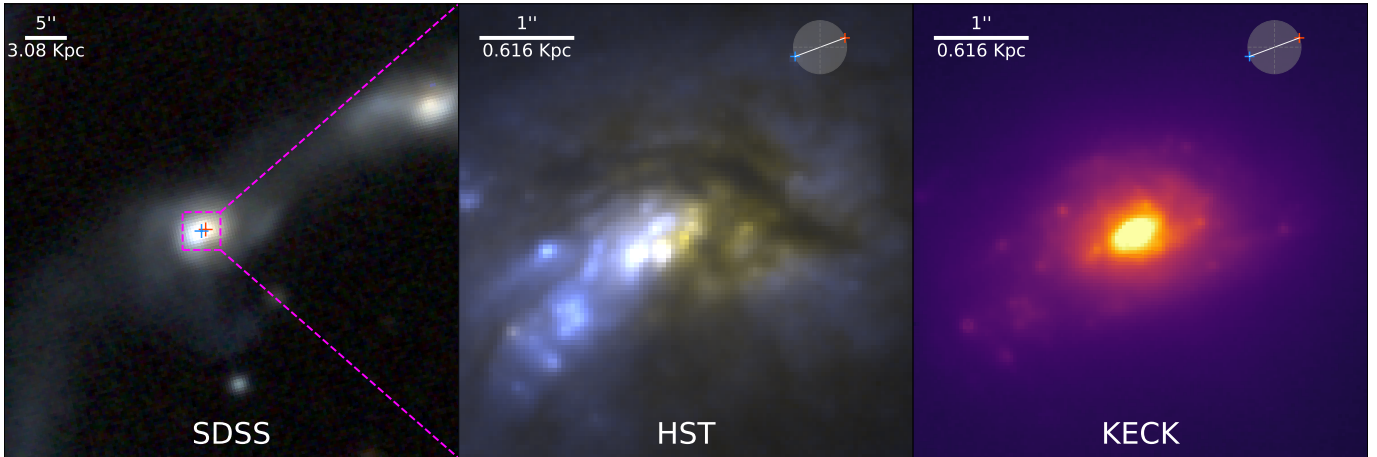
A.13. *J131534+620728*

Figure 32. Images provided above are described at the beginning of Appendix A.

J131534 is one of the targets in the 48 target Keck merger sample which has publicly available NIRC2 imaging in the Keck archive (see Section 2.1). Keck LGSAO observations of this target were conducted with the NIRC2 Wide-Field Camera (FOV: $40'' \times 40''$, pixel scale: $0.039686'' \text{pixel}^{-1}$) in the K_s ($\lambda_c = 2.146 \mu\text{m}$) filter as part of Keck observing program Z229 in 2017. Additionally, this target was included in the The Great Observatories All-Sky LIRG Survey HST sample (GOALS; Armus et al. 2009) where it was imaged with the ACS/WFC using the F435W and F814W filters (GO program 10592, PI: A. Evans). In the SDSS image we see that this target is part of an early stage merger system at a separation of $35''$ or 21.553 kpc , with the Eastern galaxy being the galaxy in which we detect an SDSS/WISE offset. The Eastern galaxy has two prominent tidal tails, one extending 24.6 kpc to the Southeast and the other connecting the two galaxies. In the NIRC2 imaging of this target we see that there is a single bright central nucleus or AGN surrounded by many sources of faint secondary emission, or substructure. Based on the criteria laid out in Section 4.2 the substructure pair we identify in this target for comparison with the SDSS/WISE offset consists of the central nucleus and a small source of emission North of the nucleus at a separation of $0.287''$ or 0.177 kpc and PA of 343.328° . The SDSS/WISE offset, with a separation of $0.585''$ and PA of 290.428° , does not appear to trace the substructure pair we define but comparison between the HST and Keck imaging reveals that the SDSS/WISE offset reflects a difference in the near-infrared and optical emission of J131517 rather than real substructure revealed by near-infrared imaging. The HST image shows that there is a significant amount of dust obscuring the Western half of the optical nuclear emission. By identifying matching sources of secondary emission visible in both the Keck and HST images we find that the central near-infrared nucleus is likely spatially coincident with the large dust cloud in the Western region of the optical nuclear emission and not the bright optical emission we see. This suggests that the SDSS/WISE offset we detect is caused by the central nucleus or AGN being obscured by dust and thus biasing the SDSS coordinate away from the true location of the AGN. The host galaxy of this object is optically classified as a K_{03} type AGN in the MPA-JHU catalog. Additionally, it lies within the composite classification of our BPT diagram and outside of the Jarrett AGN region of our WISE color-color diagram.

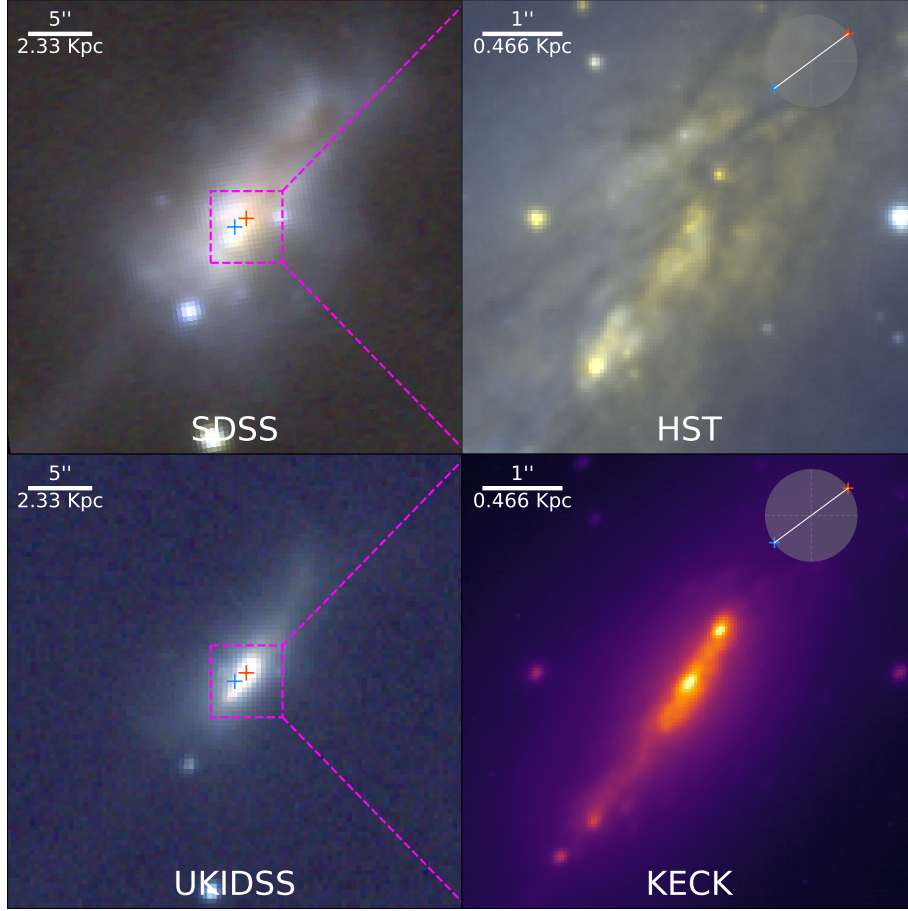
A.14. *J132035+340822*

Figure 33. Images provided above are described at the beginning of Appendix A. Note that this target does not have a UKIDSS Y band cutout image available, thus the UKIDSS three color image is comprised of K band, H band and J band images.

J132035 is one of the targets in the 48 target Keck merger sample which has publicly available NIRC2 imaging in the Keck archive (see Section 2.1). Keck LGSAO observations of this target were conducted with the NIRC2 Wide-Field Camera (FOV: $40'' \times 40''$, pixel scale: $0.039686'' \text{ pixel}^{-1}$) in the K_s ($\lambda_c = 2.146 \mu\text{m}$) filter as part of Keck observing program Z229 in 2017. Additionally, this target was included in the GOALS HST sample (Armus et al. 2009) where it was imaged with the ACS/WFC using the F435W and F814W filters (GO program 10592, PI: A. Evans). The SDSS and UKIDSS imaging of this target shows it is a highly disturbed late-stage merger with a bright and elongated central nucleus. An extended tidal tail stretching towards the Northwest is visible in both the optical and IR. Additionally, outside of the field of view of the SDSS image there are two perpendicular tidal tails, one extending 23 kpc to the Southeast and the other 29 kpc to the Southwest. NIRC2 imaging of J132035 reveals dual nuclei separated by $0.784''$ or 0.365 kpc and PA of 329.747° . Romero-Cañizales et al. (2017) confirmed the AGN nature of the central nucleus in J132035, reporting the presence of a pc-scale jet based on high-resolution VLBI observations. The secondary nucleus located to the Northwest of the central nucleus has not been confirmed as an AGN. The SDSS/WISE offset detected in the nucleus of J132035 has a separation of $1.209''$ and PA 306.487° which overpredicts the separation of the dual nuclei but has a similar orientation. The high-resolution optical HST imaging of J132035 shows that both nuclei are heavily obscured by a large dust lane visible in the SDSS image and reveals an additional bright source of optical emission in the Southeast of the HST image. It is likely that the partial obscuration of the nuclear region in J132035 is driving the SDSS/WISE offset we detect. The host galaxy of this object is optically classified as a K_{03} type AGN in the MPA-JHU catalog. Additionally, it lies within the composite classification of our BPT diagram and outside of the Jarrett AGN region of our WISE color-color diagram.

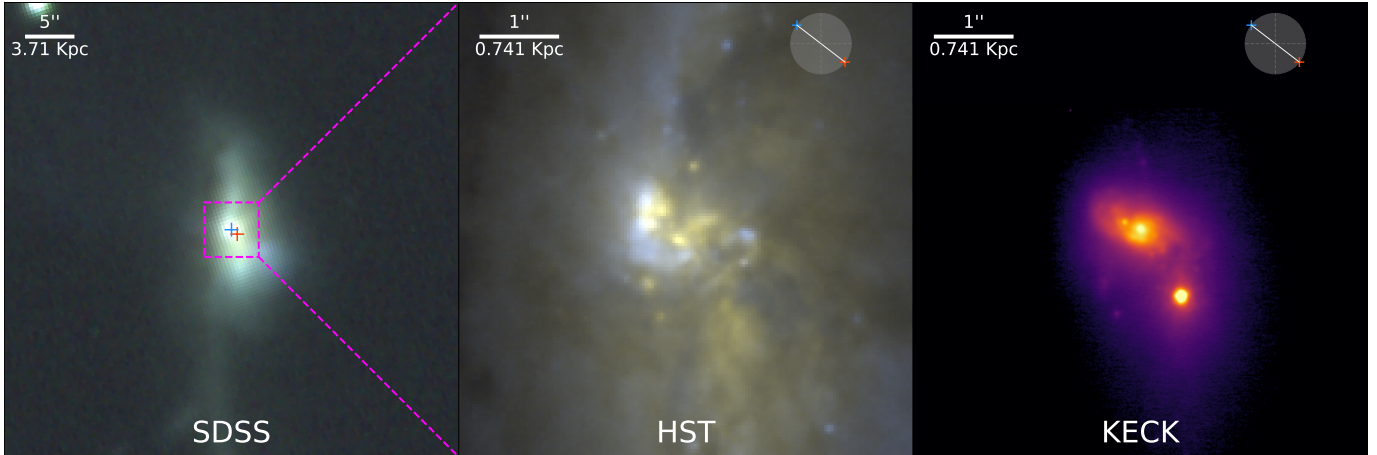
A.15. *J134442+555313*

Figure 34. Images provided above are described at the beginning of Appendix A.

J134442 is one of the targets in the 48 target Keck merger sample which has publicly available NIRC2 imaging in the Keck archive (see Section 2.1). This target is an ultra-luminous infrared galaxy (ULIRG) and late-stage merger system with a very extended optical tidal tail stretching 40 kpc to the South in the SDSS image. U et al. (2013) conducted Keck LGSAO observations of this target with the NIRC2 Narrow-Field Camera (FOV: $10'' \times 10''$, pixel scale: $0.009942'' \text{pixel}^{-1}$) in the H ($\lambda_c = 1.633 \mu\text{m}$) and K_p filters. Here we show the K_p filter image which reveals two nuclei: a nucleus surrounded by a rotating gaseous disk in the Northeast and a prominent nucleus in the Southwest at a separation of $1.035''$ or 0.767 kpc and PA of 211.969° . J134442 was confirmed to be a dual AGN system by Iwasawa et al. (2018) with follow-up NuSTAR observations which are best explained by a dual AGN system. Additionally, this target was included in the GOALS HST sample (Armstrong et al. 2009) where it was imaged with the ACS/WFC using the F435W and F814W filters (GO program 10592, PI: A. Evans). The optical HST imaging of J134442 shows a much more disturbed morphology and significant obscuration, with the Northeast AGN appearing partially obscured and the Southwest AGN being completely obscured. The SDSS/WISE offset detected in this system roughly traces the separation and orientation of the dual AGN system with a separation of $0.799''$ and PA of 232.468° (i.e. $\Delta \text{Sep.} = 0.236''$ and $\Delta \text{PA} = 20.499^\circ$). Due to the relative orientation of the SDSS/WISE offset we can see that the WISE coordinate likely coincides with the obscured Southwestern AGN and the SDSS with the Northeastern AGN, showing that the SDSS/WISE offset is likely caused by the obscuration of the optical emission of the Southwestern AGN. Additionally, due to the partial obscuration of the optical emission from the Northeastern AGN it is likely that the SDSS coordinate is not accurate to the position of the AGN and thus causing the discrepancy between the PA of the SDSS/WISE offset and dual AGN system. The host galaxy of this object is optically classified as a K_{01} type AGN in the MPA-JHU catalog. Additionally, it lies within the AGN classification of our BPT diagram and within the Jarrett AGN region of our WISE color-color diagram.

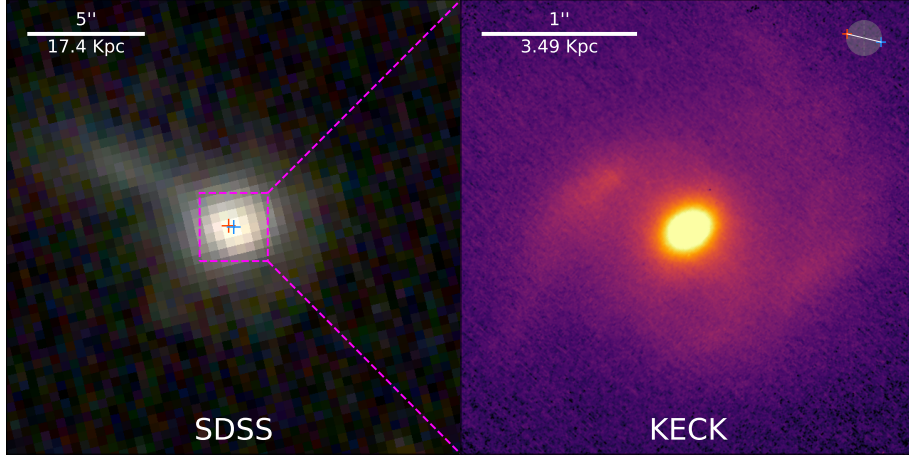
A.16. *J134651+371231*

Figure 35. Images provided above are described at the beginning of Appendix A.

J134651 appears to be a post-merger system with an extended tidal tail extending $5.5''$ or 19.19 kpc to the Northeast. The NIRC2 imaging reveals substructure in the form of apparent spiral arms in the Northeast and Southwest. In the Northeast arm we identify concentrated emission as the brightest secondary source of emission, forming a substructure pair with the central primary central nucleus with a separation of $0.633''$ or 2.209 kpc and PA of 63.589° . The SDSS/WISE offset detected in this system has a separation of $0.230''$ and PA of 76.457° which underpredicts the separation of the substructure as expected (see Section 4.2 but appears accurate to the orientation of the spiral arm relative to the central nucleus). The host galaxy of this object is optically classified as a K_{01} type AGN in the MPA-JHU catalog. Additionally, it lies within the AGN classification of our BPT diagram and outside of the Jarrett AGN region of our WISE color-color diagram.

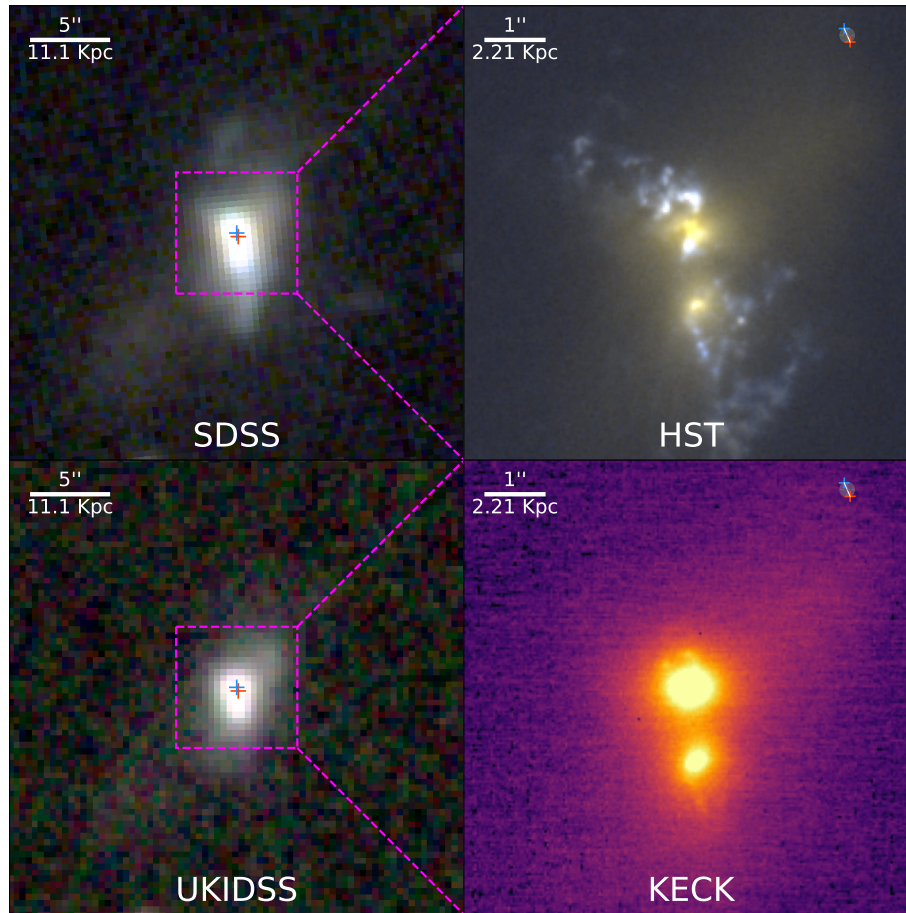
A.17. *J135646+102608*

Figure 36. Images provided above are described at the beginning of Appendix A.

J135646 is one of the targets in the 48 target Keck merger sample which has publicly available NIRC2 imaging available in the Keck archive (see Section 2.1). [Fu et al. \(2011a\)](#) conducted Keck LGSAO observations of this target with the NIRC2 Wide-Field Camera (FOV: $40'' \times 40''$, pixel scale: $0.039686''\text{pixel}^{-1}$) in the K_p filter as part of an observing program searching for kpc-scale dual AGNs in double-peaked [OIII] AGNs. Additionally, this target was included in HST F438W and F814W observations of AGN with double-peaked narrow emission lines presented in [Comerford et al. \(2015\)](#), where they identify J135646 as a candidate dual AGN. J135646 exhibits bipolar extended emission stretching ~ 15 kpc to the North and ~ 12 kpc to the South in SDSS but not in UKIDSS. Closer observations of this extended emission has found that it is likely to be a ~ 20 kpc scale outflow being driven by radiative feedback from an AGN in J135646 (e.g. [Greene et al. 2012](#)). The NIRC2 imaging of this target reveals a very bright Northern nucleus and a dimmer Southern nucleus forming a clear nuclear pair at a separation of $1.253''$ or 2.771 kpc and PA of 185.403° . The HST imaging of J135646 similarly shows two nuclei, however the optical emission of both nuclei is significantly broken up and distorted by the outflow identified by [Greene et al. \(2012\)](#). The SDSS/WISE offset detected in this system has a separation of $0.258''$ and PA of 203.430° , which is not accurate to the orientation of the dual nuclei we see in the NIRC2 and HST imaging. Based on the location of the SDSS and WISE coordinates in the SDSS and UKIDSS cutout images it is likely that the offset corresponds to the immediate vicinity of the Northern nucleus. Assuming this, it is likely that the SDSS/WISE offset is tracing the complex optical emission of the outflow near the Northern nucleus, with the WISE coordinate corresponding to the nucleus and the SDSS coordinate corresponding to the outflow. The host galaxy of this object is optically classified as a K_{01} type AGN in the MPA-JHU catalog. Additionally, it lies within the AGN classification of our BPT diagram and within the Jarrett AGN region of our WISE color-color diagram.

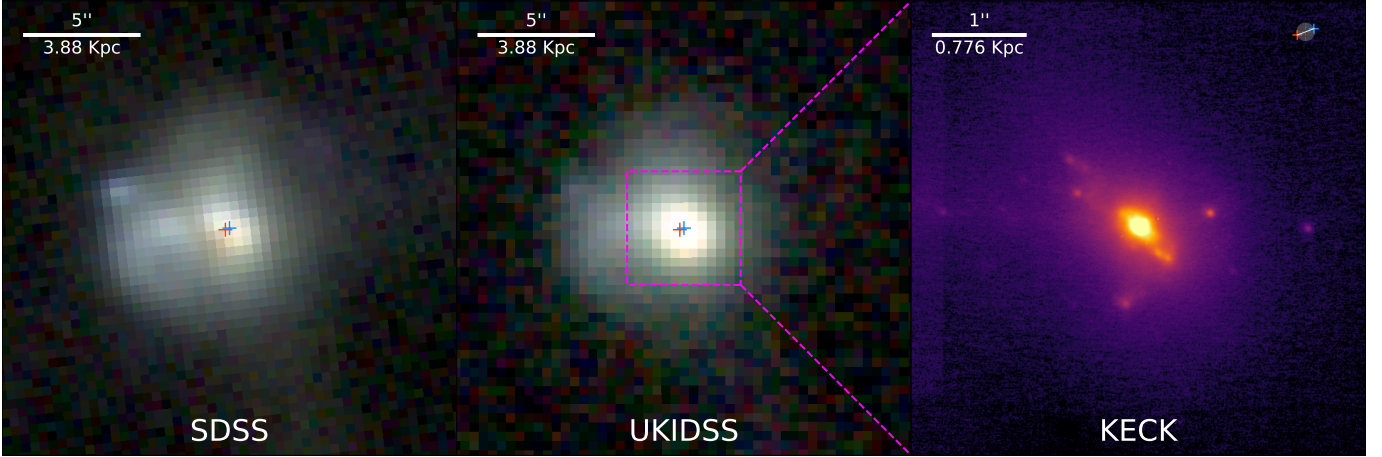
A.18. *J150517+080912*

Figure 37. Images provided above are described at the beginning of Appendix A.

J1505 is a late-stage merger system with significant tidal features and an elongated nucleus. In its SDSS image we see two tidal tails, one extending Southward out to 11 kpc and a Western tail curving Northward with an approximate length of 13 kpc. Additionally, there is a highly curved tail of emission coming out of the Western side of the nucleus looping back into the galaxy towards the South and another curved tail coming out of the Northern side of the nucleus. The NIRC2 image of this target shows multiple sources of secondary emission at sub-arcsecond separations from the central primary nucleus. The brightest of the secondaries lies at a separation of $0.347''$ or 0.269 kpc and PA of 218.893° , Southeast from the primary nucleus. The SDSS/WISE offset separation and PA are $0.194''$ and 290.978° , which does not appear to be significantly correlated to the orientation of the substructure pair. There is a dimmer secondary in the image which is separated from the primary nucleus by $0.797''$ and has a position angle of 282.239° which appears to be more consistent with the offset orientation. The host galaxy of this object is optically classified as a K_{03} type AGN in the MPA-JHU catalog. Additionally, it lies within the composite classification of our BPT diagram and outside of the Jarrett AGN region of our WISE color-color diagram.

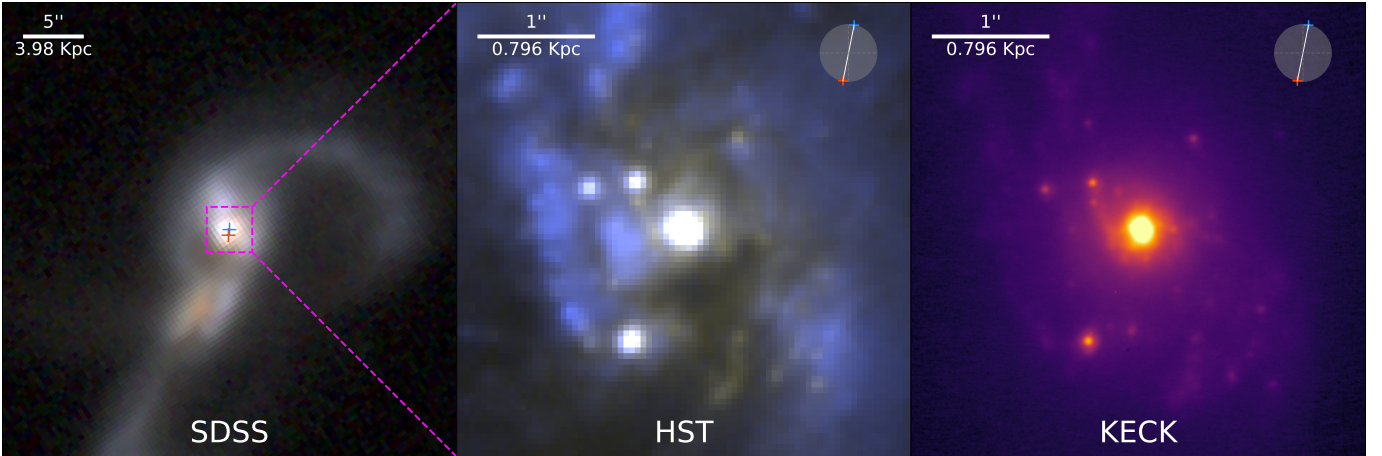
A.19. *J151806+424444*

Figure 38. Images provided above are described at the beginning of Appendix A.

J151806 is an extensively studied target also known as VV 705. The SDSS image shows that this is clearly a merging system which appears to have gone through its first pass, indicated by its very prominent tidal tails and bridge of emission between the two galaxies. This is a previously identified candidate dual AGN at a separation of 5.8 kpc based on the detection of X-ray emission in both nuclei (see Comerford et al. 2022; He et al. 2023). This target is also

included in the GOALS HST sample (Armus et al. 2009) where it was imaged with the ACS/WFC using the F435W and F814W filters (GO program 10592, PI: A. Evans). With our NIRC2 imaging we target the Northwest galaxy in which we detect an SDSS/WISE offset with a separation of $0.500''$ and PA of 168.679° . In the high-resolution NIRC2 imaging of this target, we see a bright central primary nucleus and 4 additional secondary sources of emission in the immediate nuclear region of the galaxy. Of the four secondaries the brightest lies $1.083''$ or 0.863 kpc in the Southeast from the primary with a PA of 156.010° . Together with the central primary nucleus this forms the substructure pair in J151806. In the HST images of this target we can see significant obscuration throughout the host galaxy but the same substructure can still be seen in the optical. The PA of the substructure pair is very similar to that of the SDSS/WISE offset, suggesting that the detected offset is accurately tracing the substructure in this system. The host galaxy of this object is optically classified as a K_{03} type AGN in the MPA-JHU catalog. Additionally, it lies within the composite classification of our BPT diagram and outside of the Jarrett AGN region of our WISE color-color diagram.

A.20. *J152659+355837*

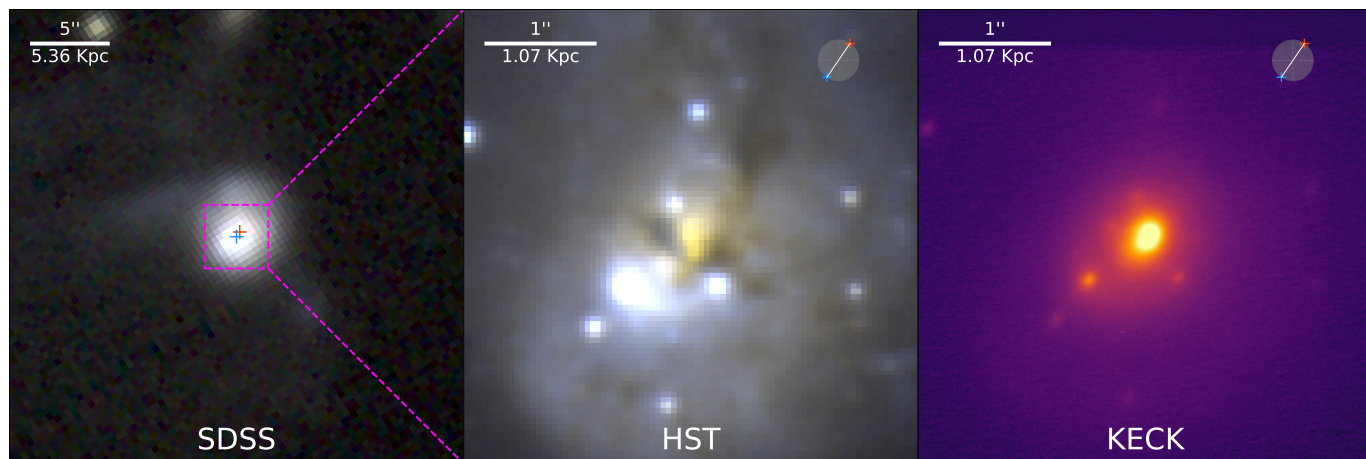


Figure 39. Images provided above are described at the beginning of Appendix A.

J152659 is an advanced merger system with tidal tails in the Southwest and East connected by an arc of emission with an approximate radius of $12''$ or 13 kpc. In the NIRC2 image we can see multiple sources of substructure within the nuclear region of this target which were unresolved in SDSS. There is a prominent bright primary nucleus in the center of the galaxy and we identify 9 different secondary sources of near-infrared emission. The brightest of these secondaries lies $0.631''$ or 0.677 kpc away from the primary nucleus with a PA of 127.543° . The SDSS/WISE offset that we detect in this system has a separation of $0.376''$ and PA of 145.649° which is relatively similar to the orientation of the substructure pair. J152659 has been studied extensively in the past at multiple wavelengths and lower resolutions with some identifying the same substructure seen in the NIRC2 image. Scoville et al. (2000) presented HST NICMOS imaging of this galaxy at $1.1\mu\text{m}$, $1.6\mu\text{m}$, and $2.2\mu\text{m}$ and identify the same pair of candidate nuclei. Scoville et al. (2000) do not classify the secondary source as a nucleus or SF region, though it is noted that the near-infrared colors of the secondary source are very red. Additionally, this target was included in the GOALS HST sample (Armus et al. 2009) where it was imaged with the ACS/WFC using the F435W and F814W filters (GO program 10592, PI: A. Evans). The same sources of secondary near-infrared emission can be seen in the optical HST imaging except for the primary central nucleus, where it is significantly obscured. When analyzed in conjunction with the orientation of the SDSS/WISE offset it appears that the WISE coordinate traces the location of the primary nucleus and the SDSS coordinate of the unobscured secondary. The host galaxy of this object is optically classified as a K_{03} type AGN in the MPA-JHU catalog. Additionally, it lies within the composite classification of our BPT diagram but is not included in the WISE color-color diagram due to it not having a listed W_3 magnitude.

REFERENCES

Agazie, G., Anumarlapudi, A., Archibald, A. M., et al.

2023, *ApJL*, 951, L8

Armus, L., Mazzarella, J. M., Evans, A. S., et al. 2009,

PASP, 121, 559

- Astropy Collaboration, Robitaille, T. P., Tollerud, E. J., et al. 2013, *A&A*, **558**, A33
- Baldwin, J. A., Phillips, M. M., & Terlevich, R. 1981, *PASP*, **93**, 5
- Bianchi, S., Chiaberge, M., Piconcelli, E., Guainazzi, M., & Matt, G. 2008, *MNRAS*, **386**, 105
- Blecha, L., Snyder, G. F., Satyapal, S., & Ellison, S. L. 2018, *MNRAS*, **478**, 3056
- Borne, K. D., Bushouse, H., Colina, L., et al. 1999, in *Astronomical Society of the Pacific Conference Series*, Vol. 177, *Astrophysics with Infrared Surveys: A Prelude to SIRTf*, ed. M. D. Bica, R. M. Cutri, & B. F. Madore, 167
- Brinchmann, J., Charlot, S., White, S. D. M., et al. 2004, *MNRAS*, **351**, 1151
- Capelo, P. R., Dotti, M., Volonteri, M., et al. 2017, *MNRAS*, **469**, 4437
- Capelo, P. R., Volonteri, M., Dotti, M., et al. 2015, *MNRAS*, **447**, 2123
- Casali, M., Adamson, A., Alves de Oliveira, C., et al. 2007, *A&A*, **467**, 777
- Chen, N., Di Matteo, T., Ni, Y., et al. 2023a, *MNRAS*, **522**, 1895
- Chen, Y.-C., Hwang, H.-C., Shen, Y., et al. 2022, *ApJ*, **925**, 162
- Chen, Y.-C., Liu, X., Lazio, J., et al. 2023b, *ApJ*, **958**, 29
- Comerford, J. M., Negus, J., Barrows, R. S., et al. 2022, *ApJ*, **927**, 23
- Comerford, J. M., Nevin, R., Stemo, A., et al. 2018, *ApJ*, **867**, 66
- Comerford, J. M., Pooley, D., Barrows, R. S., et al. 2015, *ApJ*, **806**, 219
- Comerford, J. M., Pooley, D., Gerke, B. F., & Madejski, G. M. 2011, *ApJL*, **737**, L19
- Comerford, J. M., Schluns, K., Greene, J. E., & Cool, R. J. 2013, *ApJ*, **777**, 64
- Darg, D. W., Kaviraj, S., Lintott, C. J., et al. 2010, *MNRAS*, **401**, 1043
- De Rosa, A., Vignali, C., Husemann, B., et al. 2018, *MNRAS*, **480**, 1639
- Fu, H., Myers, A. D., Djorgovski, S. G., & Yan, L. 2011a, *ApJ*, **733**, 103
- Fu, H., Yan, L., Myers, A. D., et al. 2012, *ApJ*, **745**, 67
- Fu, H., Zhang, Z.-Y., Assef, R. J., et al. 2011b, *ApJL*, **740**, L44
- Greene, J. E., Zakamska, N. L., & Smith, P. S. 2012, *ApJ*, **746**, 86
- Hambly, N. C., Collins, R. S., Cross, N. J. G., et al. 2008, *MNRAS*, **384**, 637
- Harris, C. R., Millman, K. J., van der Walt, S. J., et al. 2020, *Nature*, **585**, 357
- He, L., Hou, M., Li, Z., Feng, S., & Liu, X. 2023, *ApJ*, **949**, 49
- Hewett, P. C., Warren, S. J., Leggett, S. K., & Hodgkin, S. T. 2006, *MNRAS*, **367**, 454
- Hopkins, P. F., & Hernquist, L. 2006, *ApJS*, **166**, 1
- Hou, M., Liu, X., Guo, H., et al. 2019, *ApJ*, **882**, 41
- Hunt, L. K., & Malkan, M. A. 2004, *ApJ*, **616**, 707
- Hwang, H.-C., Shen, Y., Zakamska, N., & Liu, X. 2020, *ApJ*, **888**, 73
- Irwin, M. J. 2008, in *2007 ESO Instrument Calibration Workshop*, ed. A. Kaufer & F. Kerber, 541
- Iwasawa, K., U, V., Mazzarella, J. M., et al. 2018, *A&A*, **611**, A71
- Jarrett, T. H., Cohen, M., Masci, F., et al. 2011, *ApJ*, **735**, 112
- Kauffmann, G., Heckman, T. M., White, S. D. M., et al. 2003a, *MNRAS*, **341**, 33
- Kauffmann, G., Heckman, T. M., Tremonti, C., et al. 2003b, *MNRAS*, **346**, 1055
- Kelley, L. Z., Blecha, L., & Hernquist, L. 2017, *MNRAS*, **464**, 3131
- Kewley, L. J., Dopita, M. A., Sutherland, R. S., Heisler, C. A., & Trevena, J. 2001, *ApJ*, **556**, 121
- Kim, D. C., Yoon, I., Evans, A. S., et al. 2020, *ApJ*, **904**, 23
- Kim, M., Barth, A. J., Ho, L. C., & Son, S. 2021, *ApJS*, **256**, 40
- Komossa, S., Burwitz, V., Hasinger, G., et al. 2003, *ApJL*, **582**, L15
- Koss, M., Mushotzky, R., Treister, E., et al. 2012, *ApJL*, **746**, L22
- Koss, M. J., Blecha, L., Bernhard, P., et al. 2018, *Nature*, **563**, 214
- Koss, M. J., Treister, E., Kakkad, D., et al. 2023, *ApJL*, **942**, L24
- Lawrence, A., Warren, S. J., Almaini, O., et al. 2007, *MNRAS*, **379**, 1599
- Li, J., Zhuang, M.-Y., Shen, Y., et al. 2024, *arXiv e-prints*, arXiv:2405.14980
- Li, K., Ballantyne, D. R., & Bogdanović, T. 2021, *ApJ*, **916**, 110
- Li, K., Bogdanović, T., Ballantyne, D. R., & Bonetti, M. 2022, *ApJ*, **933**, 104
- Lintott, C. J., Schawinski, K., Slosar, A., et al. 2008, *MNRAS*, **389**, 1179
- Liu, X., Civano, F., Shen, Y., et al. 2013, *ApJ*, **762**, 110
- Liu, X., Greene, J. E., Shen, Y., & Strauss, M. A. 2010a, *ApJL*, **715**, L30

- Liu, X., Shen, Y., Strauss, M. A., & Greene, J. E. 2010b, *ApJ*, 708, 427
- Liu, X., Shen, Y., Strauss, M. A., & Hao, L. 2011, *ApJ*, 737, 101
- Liu, X., Hou, M., Li, Z., et al. 2019, *ApJ*, 887, 90
- Lyu, Y., & Liu, X. 2016, *MNRAS*, 463, 24
- Maiolino, R., Scholtz, J., Curtis-Lake, E., et al. 2023, *arXiv e-prints*, [arXiv:2308.01230](https://arxiv.org/abs/2308.01230)
- Malkan, M. A., Gorjian, V., & Tam, R. 1998, *ApJS*, 117, 25
- Marocco, F., Eisenhardt, P. R. M., Fowler, J. W., et al. 2021, *ApJS*, 253, 8
- Maschmann, D., Melchior, A.-L., Mamon, G. A., Chilingarian, I. V., & Katkov, I. Y. 2020, *A&A*, 641, A171
- McGurk, R. C., Max, C. E., Medling, A. M., Shields, G. A., & Comerford, J. M. 2015, *ApJ*, 811, 14
- Merritt, D., & Milosavljević, M. 2005, *Living Reviews in Relativity*, 8, 8
- Müller-Sánchez, F., Comerford, J. M., Nevin, R., et al. 2015, *ApJ*, 813, 103
- Perna, M., Arribas, S., Lamperti, I., et al. 2023, *arXiv e-prints*, [arXiv:2310.03067](https://arxiv.org/abs/2310.03067)
- Pfeifle, R. W., Weaver, K. A., Secrest, N. J., Rothberg, B., & Patton, D. R. 2024, *arXiv e-prints*, [arXiv:2411.12799](https://arxiv.org/abs/2411.12799)
- Pfeifle, R. W., Satyapal, S., Manzano-King, C., et al. 2019a, *ApJ*, 883, 167
- Pfeifle, R. W., Satyapal, S., Secrest, N. J., et al. 2019b, *ApJ*, 875, 117
- Pierce, J. C. S., Tadhunter, C., Ramos Almeida, C., et al. 2023, *MNRAS*, 522, 1736
- Ricci, C., Bauer, F. E., Treister, E., et al. 2017, *MNRAS*, 468, 1273
- Rodriguez, C., Taylor, G. B., Zavala, R. T., et al. 2006, *ApJ*, 646, 49
- Romero-Cañizales, C., Alberdi, A., Ricci, C., et al. 2017, *MNRAS*, 467, 2504
- Rosario, D. J., Shields, G. A., Taylor, G. B., Salviander, S., & Smith, K. L. 2010, *ApJ*, 716, 131
- Satyapal, S., Ellison, S. L., McAlpine, W., et al. 2014, *MNRAS*, 441, 1297
- Satyapal, S., Secrest, N. J., Ricci, C., et al. 2017, *ApJ*, 848, 126
- Schwartzman, E., Clarke, T. E., Nyland, K., et al. 2024, *ApJ*, 961, 233
- Scoville, N. Z., Evans, A. S., Thompson, R., et al. 2000, *AJ*, 119, 991
- Service, M., Lu, J. R., Campbell, R., et al. 2016, *PASP*, 128, 095004
- Shen, Y., Hwang, H.-C., Zakamska, N., & Liu, X. 2019, *ApJL*, 885, L4
- Shen, Y., Liu, X., Loeb, A., & Tremaine, S. 2013, *ApJ*, 775, 49
- Smith, K. L., Shields, G. A., Bonning, E. W., et al. 2010, *ApJ*, 716, 866
- Snyder, G. F., Hayward, C. C., Sajina, A., et al. 2013, *ApJ*, 768, 168
- Stasińska, G., Cid Fernandes, R., Mateus, A., Sodré, L., & Asari, N. V. 2006, *MNRAS*, 371, 972
- Taylor, M. B. 2005, in *Astronomical Society of the Pacific Conference Series*, Vol. 347, *Astronomical Data Analysis Software and Systems XIV*, ed. P. Shopbell, M. Britton, & R. Ebert, 29
- Tremonti, C. A., Heckman, T. M., Kauffmann, G., et al. 2004, *ApJ*, 613, 898
- U, V., Medling, A., Sanders, D., et al. 2013, *ApJ*, 775, 115
- Uppal, A., Ward, C., Gezari, S., et al. 2024, *ApJ*, 975, 286
- van Dam, M. A., Bouchez, A. H., Le Mignant, D., et al. 2006, *PASP*, 118, 310
- Van Wassenhove, S., Volonteri, M., Mayer, L., et al. 2012, *ApJL*, 748, L7
- Virtanen, P., Gommers, R., Oliphant, T. E., et al. 2020, *Nature Methods*, 17, 261
- Voggel, K. T., Seth, A. C., Baumgardt, H., et al. 2022, *A&A*, 658, A152
- Volonteri, M., Pfister, H., Beckmann, R., et al. 2022, *MNRAS*, 514, 640
- Volonteri, M., Pfister, H., Beckmann, R. S., et al. 2020, *MNRAS*, 498, 2219
- Wang, H.-C., Wang, J.-X., Gu, M.-F., & Liao, M. 2023, *MNRAS*, 524, L38
- Wang, J.-M., Chen, Y.-M., Hu, C., et al. 2009, *ApJL*, 705, L76
- Ward, C., Gezari, S., Nugent, P., et al. 2024, *ApJ*, 961, 172
- Wizinowich, P., Acton, D. S., Shelton, C., et al. 2000, *PASP*, 112, 315
- Wizinowich, P. L., Le Mignant, D., Bouchez, A. H., et al. 2006, *PASP*, 118, 297
- Wright, E. L., Eisenhardt, P. R. M., Mainzer, A. K., et al. 2010, *AJ*, 140, 1868
- Zhao, D., Ho, L. C., Zhao, Y., Shangguan, J., & Kim, M. 2019, *ApJ*, 877, 52